The Effect of Climate Change on the Marine Methane Hydrate Stability Zone

by

Jeremy Garmeson Fyke
B.Sc., University of Victoria, 2003

A Thesis Submitted in Partial Fulfillment of the
Requirements for the Degree of

Master of Science

in the School of Earth and Ocean Sciences

Supervisor: Dr. Andrew. J. Weaver

Abstract

The marine gas hydrate stability zone (GHSZ) is sensitive to climatically driven temperature changes at the seafloor. This thesis reviews past studies of the GHSZ response to climate change, and presents the results of a numerical analysis of a marine gas hydrate stability model forced by an intermediate complexity climate model. Potential future climate scenarios are simulated, resulting in realistic predictions of seafloor temperature change over variable bathymetry. The average continental margin seafloor temperature increase is greater than the global seafloor average, and it is determined that even for CO_2 concentrations held below present-day levels, the global GHSZ will decrease significantly. The experiments carried out here indicate that after 40 kyr the GHSZ volume will shrink by between 1% and 29%, based on various CO_2 scenarios and parameterizations of thermal diffusivity and geothermal gradient. Regions which exhibit 100% GHSZ loss range from 1% to 9% of the prescribed continental margin. Results of this study suggest that the effects of future GHSZ loss may be felt by the exogenic carbon cycle within centuries and last for tens of thousands of years.

Table of Contents

List of Tables

List of Figures

Acknowledgements

I wish to gratefully acknowledge my supervisor, Andrew Weaver, for valuable guidance and inspiration throughout my Masters program. I would also like to sincerely thank George Spence, Katrin Meissner, Mike Roth, Ed Wiebe, Mike Eby, Wanda Lewis, Jenny Brauch, Jeff Lewis, Paul Spence, Hongyan Dang, Helen Johnson and the rest of the climate lab crew for their invaluable technical and moral support, many interesting discussions, and all the fun. Finally, and most importantly, I would like to thank my family: John, Sharron (in memory), Becky and Sara.

Chapter 1

Marine Methane Hydrates

1.1 Introduction

Marine methane hydrates have attracted increasing attention in recent years due to their potential role in climate change (Dickens 2001), continental slope instability (Sultan et al. 2004) and as a future energy resource (Collett 2000). Gas hydrates are formed through the inclusion of small gas molecules into the interstices of an isometric crystal ice lattice under suitable pressure, temperature and solubility conditions (Kvenvolden 1993). In the marine setting, high pressure and low temperatures within the seafloor allow methane hydrates to form, given sufficient gas and water supply (Dickens 2001). Terrestrially, methane hydrates may exist in high latitude continental regions due to cold subsurface temperatures (Collett and Dallimore 2001).

Due to the supply of methane from the anaerobic breakdown of organic material within seafloor sediments, methane Structure I hydrates dominate the natural marine gas hydrate reservoir (Sloan 2003). Continental margins appear to contain the majority of the marine methane hydrate inventory, due to increased organic input from terrestrial debris, upwelling (Gornitz and Fung 1994), as well as gas and fluid flux expulsion from pelagic sediments during active subduction (Hyndman et al. 1993). Several studies have quantified the global extent of marine gas hydrates using various techniques (see Milkov (2004) for a comprehensive review). Current published values for the volume of the marine gas hydrate stability zone (GHSZ) and the mass of carbon stored as hydrate within it lie between 5-31.2 x 10^6 km^3 and 100-74400 Gt C (Milkov 2004, Soloviev 2002, Klauda and Sandler 2005), with the wide range of stored carbon values resulting from the particular geographical, sedimentary and geochemical constraints utilized by various studies.

The volume of the marine GHSZ is dependent upon external conditions, particularly hydrostatic pressure and seafloor temperature, that determine the depth to the base of the hydrate stability zone (BHSZ). Accordingly, several studies have investigated the effect of changes to sea level and seafloor temperature on the methane hydrate reservoir in order to gauge the sensitivity and response of the marine GHSZ to climate change. Xu et al. (2001) modelled potential changes to the flux of methane from the seafloor in response to temperature and pressure perturbations for both the Paleocene/Eocene Thermal Maximum

(PETM) and the present day, using the hydrate model of Xu and Ruppel (1999). Katz et al. (2001) modelled the GHSZ response to PETM warming using model parameters based on ODP site 1051, while Dickens (2003) considered the carbon capacitor behaviour of the marine gas hydrate reservoir under changing external conditions. Such studies have typically applied idealized temperature changes to modelled GHSZs, thereby ignoring the regional GHSZ response to realistic seafloor temperature perturbations over variable bathymetry.

To address this shortcoming, I utilize the intermediate complexity UVic Earth System Climate Model (ESCM) to undertake a series of sensitivity experiments in which spatial and temporal changes to the global GHSZ in response to potential future climate change are explored.

1.2 Marine gas hydrates

1.2.1 Chemistry and Thermodynamics

Gas hydrates potentially occur within a range of pressures and temperatures and with sufficient gas and water supply. The three phase (gas, hydrate and water) equilibrium curve (henceforth the 'equilibrium curve') forms the basis upon which further study of hydrate stability takes place. The equilibrium curve designates the transition between co-existing hydrate and fluid, and co-existing gas and fluid. As can be seen in Figure 1.1, an isothermal increase in pressure or an isobaric decrease in temperature will promote hydrate stability, and when a generic equilibrium curve is overlaid with a typical temperature-depth profile of the water column and shallow seafloor, potential gas hydrate stability zones (GHSZ) are apparent. Particularly, gas hydrates may be thermodynamically stable within the lower water column and at depths of up to several hundred meters into the seafloor.

Gas hydrate equilibrium curves for both fresh and saline waters have been calculated by multiple authors (for review see Peltzer and Brewer (2000)) using several different techniques. Primary to many methods is the empirical curve-fitting of data acquired through growth and dissociation of hydrates under controlled conditions (Figure 1.2). Fits are then extrapolated to pressure-temperature regimes that encompass plausible natural conditions if these conditions are not met in the laboratory. Once initial equilibrium curves are determined, the effect of additional environmental parameters secondary to temperature and pressure may be studied. As the degrees of freedom increase with each additional parameter added, comprehensive laboratory studies of hydrate stability conditions with all possible combinations of parameters are effort-intensive and hence most studies focus on the variation of one or two parameters while holding all others fixed. Parameters that significantly affect the position of the equilibrium curve in P-T space include composition of pore waters (Dickens and Quinby-Hunt 1997), composition of source gas (Klauda and Sandler 2002), and sediment composition and pore structure (Clennell 2000).

Gas hydrates will form under proper P-T conditions only if the environment is saturated with respect to the gas mixture. Once the gas concentration has reached the pressure-

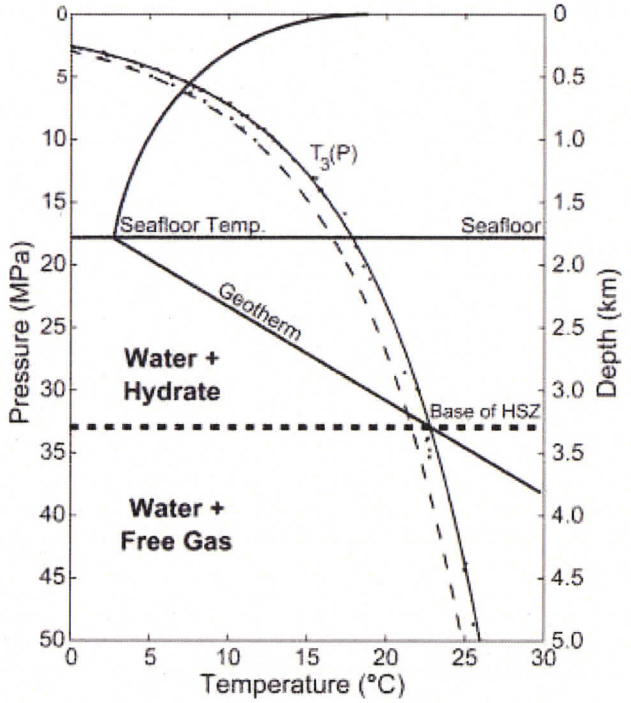

Figure 1.1: Hydrate equilibrium curves overlain by a schematic ocean/sediment temperature profile. Solid/dashed lines represent equilibrium curves in pure/sea water (Buffett and Archer 2004).

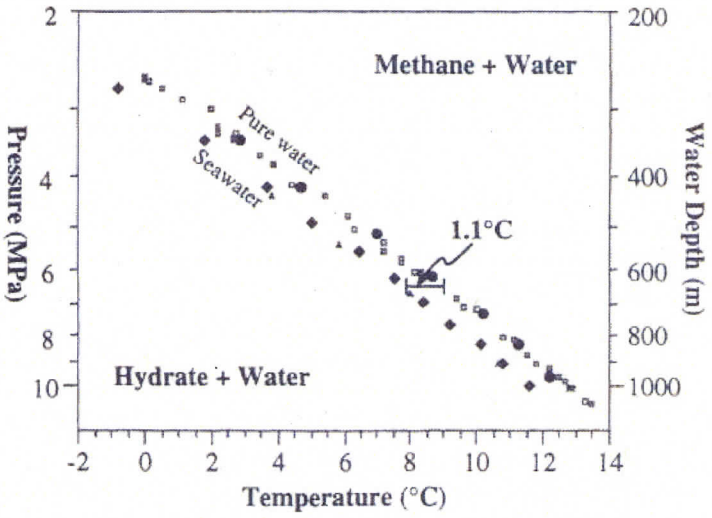

Figure 1.2: Observations of methane hydrate formation/dissociation at various pressures and fluid types (circles, hashes = pure water, diamonds, triangles = seawater), (Dickens and Quinby-Hunt 1994).

and-temperature-dependent solubility point, the gas concentration remains constant and hydrates are formed (Xu and Ruppel 1999). If the gas concentration remains below the solubility line, hydrates will not form despite favorable P-T conditions. As ocean water is vastly undersaturated with respect to the predominant hydrate-forming gases, any steady-state occurrence of hydrates in the water column is very unlikely.

The process of gas hydrate formation/dissociation produces changes in temperature and pressure due to latent heat and phase-change effects. 1 m^3 of methane hydrate hosts 164 m^3 of methane gas at STP (Kvenvolden 1998) so that if significant amounts of hydrate dissociate within a sediment column, overpressuring will occur. The latent heat absorbed during methane hydrate dissociation into vapor and liquid $\Delta H_d = 54.2$ KJ/mol (Sloan 1998); dissociation will tend to cool the local environment. Both pressure and temperature effects associated with phase change therefore act to prevent further hydrate formation/dissociation.

The stability and structure of natural gas hydrates depends largely on the source gas (Sloan 1998). Source gases with small molecular radii, such as CH_4 or CO_2, form Structure I hydrates consisting of 46 water molecules and (at most) 8 gas molecules per unit cell (Sloan 2003). The addition of significant proportions of larger gas species (for example, propane and higher hydrocarbons) will result in the formation of Structure II and Structure H hydrates (Pohlman et al. 2005, Sassen et al. 2005). Due to source gas formation through thermogenic breakdown of organic matter, II and H hydrates are termed thermogenic hydrates; these hydrates are stable to much greater depths given similar external conditions (e.g. Milkov and Sassen (2000)).

Due to the predominance of biogenic methane as a natural source gas, Structure I hydrates are thought to dominate the marine hydrate reservoir (Kvenvolden 1998). Biogenic methane is created through anaerobic microbial breakdown of organic matter and can form within the GHSZ or be delivered through expulsion of fluid during compaction within the accretionary wedge of convergent margins (Hyndman and Davis 1992) or rapid sedimentation (Gornitz and Fung 1994). In-situ methanogenesis requires enough organic matter fuel to saturate the GHSZ with methane (Gornitz and Fung 1994). For this reason areas of significant methane hydrate occurrence likely correspond to regions of high sediment organic matter content. Such conditions are most easily met along intermediate depths of continental margins where upwelling, high primary productivity and continental runoff provide large fluxes of organic matter to the seafloor. Additionally, margin sedimentation rates are typically higher and depths are shallower than in the abyssal ocean which allows more organic carbon rain to reach the seafloor instead of being oxidized within the water column. Another important factor that regulates sub-surface organic carbon concentration is the aerobicity of sea water at the seafloor (Buffett and Archer 2004): oxic seawater will act to oxidize organic matter resting at the seafloor before it can be preserved through burial.

As the marine gas hydrate reservoir is dominated by methane, further discussion will

be devoted to methane hydrates, as opposed to the more general gas hydrates. The caveat that the marine gas hydrate reservoir does contain thermogenic gases, with significantly different properties than those of purely methane hydrate, must be recognized.

1.2.2 Observation of marine gas hydrates

The observation of marine gas hydrates relies largely on indirect methods due to the inherent instability of gas hydrates outside the GHSZ. A common means of inferring hydrate presence is through seismic observation of a prominent subsurface seismic polarity reversal, commonly called the bottom-simulating reflector (BSR) (Figure 1.3).

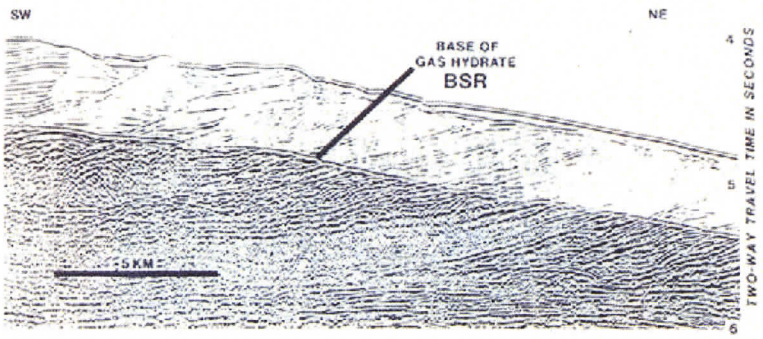

Figure 1.3: A prominent BSR observed on Hydrate Ridge. Notice the cross-cutting of the BSR with respect to other prominent reflectors. The blanking in the upper section is likely due to the presence of gas hydrates (Kvenvolden 1998).

This horizon is assumed to result from the negative density contrast between overlying hydrate-filled sediments and the underlying free gas layer; for this reason it is often assumed to mark the bottom of the GHSZ. BSRs have been observed along many continental margins (e.g. Miller et al. (1991), Hyndman and Spence (1992), Foucher et al. (2002), Bangs et al. (2005)) and are often used as the primary indicator of gas hydrate.

There are several other techniques used to infer the presence of gas hydrate. Anomalously fresh pore water in sediment cores is often used as an indication of hydrates because dissociation during coring releases fresh water originally sequestered in hydrate ice (e.g. Lange and Brumshack (1998)). In-situ down-core logs of sonic velocity, porosity and resistivity can identify important factors associated with hydrate including changes in bulk shear strength, pore percent and composition (Goldberg et al. 2000). Infrared photographs of recently retrieved core barrels have identified cold regions of the core associated with endothermic melting of pockets of hydrate (Weinberger et al. 2005). Direct observation of hydrates in the natural environment is rare: occasionally exposed hydrate is observed on the seafloor or retrieved from cores before it dissociates.

1.3 Marine methane hydrates and climate change

The depth to the BHSZ as well as methane solubility within the GHSZ can be affected via changes in temperature and pressure. Changes in temperature within the GHSZ may originate from variations in the temperature of seawater at the seafloor, although significant thermal changes in the seafloor may occur through shallow-lithosphere magmatic intrusions and associated hydrothermal activity (Svensen et al. 2004). Changes in pressure are derived from changes in hydrostatic and lithostatic pressures within the sediment column which, in addition to sea level change, can be affected through tectonic activity, sedimentation rate and overlying sediment mass movement.

1.3.1 Past climate change

Quaternary climate change

Late Quaternary climate has been dominated by periodic glacial/interglacial periods that appear to mirror variations in the Earth's orbital parameters (Milankovitch cycles). Such cyclicity is observed in ice cores in Greenland and Antarctica dating back 740 kyr (Petit et al. 1999, Augustin et al. 2004, Andersen et al. 2004) in which regular variation in temperature (inferred through $\delta^{18}O$ and $\delta^{2}D$ isotopic proxies) is largely paralleled by preserved CO_2 and CH_4 concentrations. As the temperature change cannot be solely accounted for by slight seasonal changes in incoming radiation resulting from variations in the Earth's orbit around the sun, it has been proposed that one or more feedback mechanisms within the Earth's climate system must magnify the solar forcing perturbations, resulting in the large-scale glacial/interglacial fluctuations. In particular, processes that regulate the concentration of important greenhouse gases in the atmosphere are thought to provide important feedback mechanisms and it has been suggested that changes in the marine methane hydrate reservoir may be one such mechanism. Kennett et al. (2003) argue that marine hydrates responding to changes in ocean circulation during sea level lowstands acted as triggers for abrupt post-glacial (post-Younger Dryas and Preboreal) and millenial-scale warming events. They hypothesize that during glacial periods continental margin bottom water temperatures were colder, allowing significant hydrate accumulation. When bottom water temperatures warmed, the accumulated hydrates became unstable and periodically released, warming the atmosphere and initiating other positive feedback mechanisms (i.e CO_2 expulsion from warming ocean waters and melting of permafrost). Large negative benthic foraminiferal $\delta^{13}C$ excursions associated with rapid warming provide evidence for this hypothesis, as the proposed marine methane hydrate release would have provided a large pulse of depleted carbon to the ocean interior. Maslin et al. (2004) attempted to correlate periods of increased continental slope failure (attributable to marine methane hydrate dissociation, sediment overpressuring and failure) to periods of high atmospheric methane during the Quaternary. Their findings supported the hypothesis of Kennett et al. (2003) for glacial-interglacial transitions but not for the more frequent millenial-scale climate cycles, for which they observed

no increase in frequency of continental slope failures.

The correlation between temperature and CH_4 in ice cores is an important constraint on the theory of Kennett et al. (2003). In order for temperature to significantly affect the marine GHSZ, a temperature pulse must first diffuse through the sediments to the BHSZ. The thermal timescale may be approximated as:

$$t = D^2/\kappa \tag{1.1}$$

where t is the characteristic timescale taken for a thermal pulse to reach depth D below the seafloor and κ is seafloor thermal diffusivity. For typical values of D and κ, $t \approx 10^3$-10^4 years, implying that a substantial delay should exist between initial warming and large-scale methane release from marine hydrates. In virtually all ice records, offsets between changes in temperature, CH_4 and CO_2 are smaller than the temporal resolution of the analytical methods. In an effort to determine the temperature/CH_4 offset, Severinghaus et al. (1998) utilized an isotopic technique to account for the averaging that occurs during gas diffusion within the upper firn layer of a Greenland ice core. They suggested that atmospheric methane increase lagged changes in surface temperature by 0-30 years during rapid warming from the last glacial period. This is orders of magnitude smaller than the millenial-scale lag expected for the marine hydrate reservoir, suggesting that it is not the dominant regulator of methane over glacial and millenial timescales. Additional lines of evidence conflict with the theory of Kennett et al. (2003). For example, the build-up timescale of hydrates is $\sim 10^6$ years (Archer and Buffett 2005). If the hydrate reservoir were to destabilize and release on a global scale it would take this long for the 'capacitor' to recharge and it is therefore difficult to call for periodic global-scale releases of methane on 10^3-10^5 year timescales.

Paleocene-Eocene Thermal Maximum (PETM)

The Paleocene-Eocene Thermal Maximum was a period of rapid climate change that included rapid high-latitude deep-sea temperature increase, a large negative $\delta^{13}C$ excursion and major extinctions of intermediate-to-deep sea benthic fauna (Kennett and Stott 1991, Zachos et al. 2003). It has been suggested that large-scale deep-ocean warming occurred due to a sudden switch of high-latitude deep water formation sites from southern to northern hemispheres (Bice and Marotzke 2002), and that this temperature increase destabilized a large portion of the GHSZ. Isotopic mass-balance calculations using a simplified global carbon cycle model (Dickens et al. 1997) suggest that a release of 1120 Gt hydrate-derived CH_4 with a $\delta^{13}C$ of -60 permil could have caused the global carbon isotope excursion.

Xu et al. (2001) modelled the effect of an idealized temperature perturbation on methane flux from the seafloor using a single-column sediment/methane hydrate model that included coupled equations of mass, momentum, energy and methane transport. When background seafloor temperatures were set at 11°C (simulating typical PETM conditions) and a 4°C perturbation was applied, a significant increase in the flux of methane from the seafloor

resulted as the GHSZ shallowed. Katz et al. (2001) used a time-dependent heat diffusion model to model the change in the GHSZ and compare it to $\delta^{18}O$ measurements recorded by benthic foraminifera and the global $\delta^{13}C$ perturbation noted in many records. They hypothesized that a significant $\delta^{18}O$ decrease (indicating a rise in seafloor temperature) should precede the carbon isotope excursion by at least 2300 years to allow time for complete GHSZ loss along continental margins.

An alternate hypothesis explaining the PETM warming and isotope excursion implicates the intrusion of magma into organic-rich sedimentary strata, which could have produced massive amounts of thermogenic methane within the contact aureoles of the sills (Svensen et al. 2004). These authors correlate the intrusion of a large melt complex into organic-rich mudstones of the Møre and Vøring basins in the Norwegian Sea with the PETM excursion, and calculate that enough methane could have been formed through thermogenic cracking to produce the PETM isotope signature.

1.3.2 Future climate change

Anthropogenic fossil fuel emissions are currently contributing to an increase in atmospheric greenhouse gases, particularly CO_2 (Houghton et al. 2001). Predictions of future greenhouse gas concentrations depend on anthropogenic emission scenarios which are subject to considerable uncertainty. However, even with the most optimistic scenarios, CO_2 concentrations are expected to increase for at least the next several decades before stabilizing at considerably elevated levels (Houghton et al. 2001). Draw-down of atmospheric CO_2 over millenial timescales will be governed by carbon storage in the deep ocean, with a timescale regulated largely by the rate of oceanic overturning and biological carbon sequestration (the 'inorganic' and 'organic' carbon pumps, respectively). Ewen et al. (2004) modelled anthropogic CO_2 drawdown using the UVic Earth System Climate Model with a carbon solubility pump model, and found that the inorganic carbon pump has the capacity to take up 65-75% of the anthropogenic CO_2 over a period of several thousand years. After the point at which the $CaCO_3$-buffered ocean-atmosphere carbon reservoir has reached equilibrium, silicate weathering slowly sequesters carbon such that residual excess CO_2 will remain in the atmosphere for up to 500 kyr (Archer and Ganopolski 2005).

Numerous studies indicate that increasing greenhouse gas concentrations raise the surface temperature of the Earth, driving many aspects of the climate system to new equilibrium states. Of particular relevence to the marine GHSZ is the potential future response of ocean temperature and sea level.

Ocean temperature

Temperature in the interior of the ocean experiences a delayed response to changes in surface temperature due to the time required for heat to be diffused and advected to depth. The rate of temperature change in the deep ocean is roughly tied to the overturning timescale of the thermohaline circulation (THC) which is a partial function of atmospheric CO_2 (Stouffer

and Manabe 2003). The characteristic overturning timescale of the ocean is on the order of 10^3 years, and so changes to globally averaged seafloor temperature are expected to act on approximately the same timescale. However, the response time will lessen for shallower seafloor depths, particularly those in contact with the upper mixed layer of the ocean. In these regions heat can be effectively mixed to depth, although this effect likely decreases as the water column stratifies in response to surface warming.

Predictions of future ocean temperature rely largely on climate models. Barnett et al. (2005) compared observations of ocean warming since 1960 to climate models forced with both internal and external variability (volcanics and solar activity), and greenhouse gas and sulphate aerosol forcing. They found a clear correlation between anthropogenically-forced runs and observed ocean temperatures to depths of up to 700 m, indicating that current ocean warming is caused by increases in absorption of heat at the ocean surface due to anthropogenic emissions. Stouffer and Manabe (2003) used a climate model to investigate the response of the thermohaline circulation to changes in atmospheric CO_2. As part of their analysis they studied the increase in temperature of the ocean at 3 km depth, and found that during 2x/4x current CO_2 equilibrium experiments the deep ocean warmed by 3.4/5.5°C after several thousand years.

Sea level

Houghton et al. (2001, chap. 11) reported upon long-range scenarios of sea level rise resulting from thermal expansion and the melting of continental ice sheets. As thermal expansion alone does not contribute significantly to a change in hydrostatic pressure at the seafloor, the effect of ice sheet melt must be considered separately. The largest repositories of continental ice occur on the Greenland and Antarctic ice sheets, and the future response of these large ice masses will largely determine the ice-melt contribution to sea level rise. The Greenland Ice Sheet (GIS) is the most vulnerable to climate warming (Houghton et al. 2001, chap. 11): it is predicted that the ice sheet could not survive (except for residual high glaciers) for annual average temperature increases of more than 2.7°C, and most long-term SRES scenarios exhibit warming over Greenland of much more than this value. Ridley et al. (2005) utilize a climate model coupled to a high-resolution ice sheet model to study the response of the GIS to future increases in atmospheric CO_2. They find that under 4x present day CO_2 conditions, the GIS is almost totally melted after 3000 years. Such total melting of the Greenland ice cap would contribute 6-7 m to global sealevel. The West Antarctic ice sheet (WAIS), considered the most sensitive region of the Antarctic ice mass to climate change, could theoretically contribute another 6 m to global sea level rise (Houghton et al. 2001, chap. 11). Increased precipitation and storage on the WAIS during the next century may in fact contribute to a slight decrease in sea level. However, it has been suggested that the WAIS may disintegrate over the next 5-7 hundred years in response to warming of a few degrees (Houghton et al. 2001, chap. 11), but this prediction relies on ice flow rates that are much greater than those observed today. A worst-case scenario, combining the total

melting of both the GIS and the WAIS, results in a 12 m sea level rise within the next millenia.

1.4 Previous marine methane hydrate modelling studies

The current extent of the marine gas hydrate reservoir and its potential response to climate change has motivated several studies. Various methods have been used to simulate the marine GHSZ, methane hydrate reservoir and the link between marine methane hydrates and the global carbon/climate cycle; these methods range from detailed mechanistic models to idealized carbon cycle experiments. Mechanistic models typically aim to study the dynamics of the hydrate system, either in steady state or in response to idealized external perturbations. Such models therefore invest heavily in components such as coupled equations of multi-phase fluid flow, heat flow, diffusion of pressure perturbations and parameterizations of sediment structural strength. While such studies are invaluable in gaining insight into the dynamics of the hydrate system, they are not typically coupled to 3-D climate models or detailed observational environmental data. Other studies sacrifice hydrate model complexity in order to feasibly study the sensitivity of the hydrate reservoir to climate change. Often, the GHSZ is modelled as a function of external pressure and temperature forcings, and hydrate 'filling' of this volume is calculated using a simplified set of constraints (e.g. surface chlorophyll content, surface sediment carbon content, or bathymetry). As the carbon contained within methane hydrates may enter and affect the exogenic carbon reservoir, several studies use either mechanistic or simplified hydrate models coupled to atmospheric radiative models to determine the potential feedback of hydrates to past and future climate change.

Gornitz and Fung (1994) present potential equilibrium distributions of marine methane hydrates based on maps of geothermal heat flow, satellite-derived sea surface chlorophyll content, Levitus (1982) seafloor temperature and depth and both in-situ and fluid-flow models of methane hydrate formation. The in-situ model assumes that all methane is formed by microbial methanogenesis within the GHSZ, resulting in an even filling of pore space from the seafloor to the BHSZ. This model is constrained by surface chlorophyll concentrations. The fluid-flow model assumes that all methane is generated below the GHSZ and advected upwards where it forms hydrate. The horizontal extent of hydrate occurrence in this model is confined to active (accreting and non-accreting) margins and regions of passive margins that experience high sedimentation rates; it predicts a greater concentration of hydrate at or near the BHSZ and produces a hydrate distribution that better represents observed deposits. They suggest that the in-situ hydrate formation model is more prone to destabilization because of it generally occurs under shallower and warmer seafloors compared to the fluid-flow model, and that the character of the global hydrate reservoir is likely a combination of the two models.

Harvey and Huang (1995) describe a model that resolves a 1°x1° methane hydrate reservoir using datasets of bathymetry, seafloor temperature, geothermal heat flow and

sediment organic carbon content. They then apply output from a one-dimensional, globally averaged atmosphere-ocean model (driven by step-function surface temperature increases) to a set of equations describing the rate of change of temperature and methane concentration within each column to gauge the response of the methane hydrate reservoir. Important features of their model include an estimate of the horizontal extent of the marine methane hydrate reservoir based on present-day organic carbon content distributions in the world oceans and a 'critical temperature difference' of less than 10°C at the seafloor. This refers to the temperature increase needed to destabilize hydrate at the seafloor and thereby allow gas to escape to the ocean without being re-precipitated as hydrate. Their thermodynamic model takes into account the diffusion of temperature perturbations from the seafloor and the latent heat change associated with the endothermic hydrate dissociation process. They examine two scenarios, one in which methane is released through diffusion and another in which methane can escape rapidly once enough pressure is developed through hydrate-sourced gas formation. In the diffusive case methane can only be released to the environment once the entire GHSZ is lost (i.e. once the critical temperature is reached). Under their simplifying assumptions, they find that 98% of the marine hydrate occurs in sediments where this critical temperature difference exceeds 4°C. They find that the climate feedback factor $f_{clathrate}$ increases with increasing warming such that for greater warming, proportionally more methane is dissociated. Their primary conclusion is that uncertainty in future climate warming is greater than the uncertainty in the hydrate response.

Xu and Ruppel (1999) detail a mechanistic, steady-state model of the marine methane hydrate reservoir that involves coupled equations of conservation of momentum, fluid mass, energy and methane gas in a vertical (one-dimensional) system. They find that the zone of actual methane hydrate occurrence depends largely on the availability of methane in excess of its solubility in seawater. The mass fraction of methane varies with depth and fluid flow: as fluid transports methane through the GHSZ it becomes methane-depleted as methane is sequestered as hydrates. Once the methane concentration in the rising fluid passes below the temperature-and-pressure-dependent methane solubility line no more hydrate forms and the methane concentration remains constant (assuming no other sinks such as sulfate reduction). This implies that except for extremely methane-rich systems or systems with rapid fluid flow, no hydrate is expected at the seafloor. Due to the dependance of the methane solubility curve on pressure and temperature a no-hydrate zone may exist at the bottom of the GHSZ and a gas-and-hydrate free zone may separate the underlying free gas zone from the bottom of the GHSZ. Fluid flow strongly affects both the zone of actual hydrate occurrence and the GHSZ. For a given fluid flux, an increasing methane flux allows hydrate formation at higher solubilities thereby deepening the base of the zone of methane occurrence to a maximum depth equal to the BHSZ depth. This is contrary to the common assumption that hydrate always forms at the BHSZ: this only occurs if the methane mass fraction below the BHSZ is higher than the local methane solubility. They also find that

advective methane transfer is able to build a steady-state hydrate reservoir at a much more rapid rate that a gradual diffusion-dominated system and therefore suggest that any sizeable methane hydrate deposits (for example, Blake Ridge or those off the Cascadia Margin) occur in regions of advective methane transport.

Xu et al. (2001) provide a model, based on the equations of Xu and Ruppel (1999), to study the response of a methane hydrate layer under a 1200 m-deep water column to idealized changes to seafloor temperature and pressure. They find that while realistic pressure perturbations (up to 1 MPa or ~100 m water) affects the hydrate reservoir negligibly due to a weak dependance of methane solubility on pressure, perturbation of present-day bottom water temperatures (3°C) with a 4°C seafloor temperature increase strongly affects both the GHSZ and the hydrate reservoir, with the latter being primarily due to a strong temperature-solubility dependence. However a significant change in the concentration of methane at the seafloor only occurs 10 kyr after the surface temperature pulse.

Dickens (2001) present an idealized model of the equilibrium global GHSZ, and study variations to this volume due to changes in prescribed continental slope geometries, pore-water activities (corresponding to dissolved salts in pore water), geotherms and seafloor temperatures. He finds that the potential gas hydrate volume (i.e. the pore space existing within the prescribed GHSZ) has likely increased in the last 100 Ma due to gradual seafloor cooling, but that rapid warming spikes such as the PETM periodically reduced the GHSZ significantly, potentially releasing methane to the exogenic carbon cycle. This study neglected the dynamics and thermodynamics of the methane hydrate system covered in the previous examples, but for million-year trends of the global GHSZ this is probably appropriate.

Buffett and Archer (2004) describe a mechanistic model for the distribution of marine methane hydrates and use it to determine the change in the steady-state inventory to temperature changes at the seafloor. Unique in their model construction is the use of bottom water O_2 concentrations in conjunction with a sediment diagenesis model to constrain organic carbon content in the sediment, which is then applied to a steady-state hydrate model. Prescribed changes in seafloor temperature are used to determine the difference in steady state hydrate inventories: is was found that when a 3°C temperature increase was applied the global hydrate inventory decreased by 15%. This decrease is attributable to a decrease in the GHSZ and an increase in the organic carbon needed to saturate sediments through microbial methanogenesis. They suggest that the largest sources of uncertainty in their study involved the efficiency of organic carbon matter conversion to methane and the rate of vertical fluid flow.

Archer and Buffett (2005) analyse the response of the steady state hydrate model of Buffett and Archer (2004) to an anthropogenically-induced temperature pulse to the ocean floor. They divide the hydrate reservoir into two parts: one that releases methane catastrophically (i.e on timescales of 1-100 kyr, roughly paralleling the time taken for the GHSZ

to decrease and methane to outgas through sediment failure) and the other that releases over Myr timescales (i.e. through gradual diffusion). They find that the potential feedback strength of the marine hydrate reservoir is strongly dependent on the (prescribed) fraction of hydrates that responds catastrophically and the magnitude of the catastrophic release timescale. Furthermore, they suggest that during interglacials release of methane from hydrates was small due to the lack of recharge of the hydrate capacitor. However, they suggest that the effect of future warming may potentially release thousands of Gt C as the Earth moves into a thermal state that is unprecedented over the Myr timescale of hydrate growth.

1.5 Present study

The study presented in this thesis utilizes the intermediate complexity University of Victoria Earth System Climate Model (UVic ESCM) to simulate global seafloor temperatures and changes to this field over time in response to potential future climate change. Simulated seafloor temperatures and hydrostatic pressure gradients (derived using model ocean depths and prescribed steric sea level rises) are used to drive a thermal diffusive model of the seafloor, which is used to calculate the global GHSZ. The advantage of this model configuration is that regional and temporal variations in the GHSZ, as a function of physically realistic future climate scenarios, can be modelled. The model is described in greater detail in Chapter 2, and results are presented in Chapter 3 and summarized in Chapter 4.

Chapter 2

Methodology

2.1 The UVic ESCM model

2.1.1 Background

This study uses Version 2.7 of the intermediate complexity UVic ESCM. The UVic ESCM couples a 3-D ocean general circulation model, a 2-D atmospheric model, a thermodynamic/dynamic sea ice model, and a land surface model. It is described in detail in Weaver et al. (2001). All components have a zonal resolution of 3.6° and a meridional resolution of 1.8°. The UVic ESCM is forced from start-up to equilibrium by variations in insolation and surface winds. Heat and freshwater are conserved to machine precision without the use of flux adjustments.

The ocean component is version 2.2 of the Geophysical Fluid Dynamics Laboratory Modular Ocean Model (Pacanowski 1995). It has 19 vertical levels that increase parabolically in thickness from 50m at the surface to 518m at depth. The vertical diffusivity is a function of depth according to the scheme of Bryan and Lewis (1979). Mixing associated with mesoscale eddies is parameterized according to Gent and McWilliams (1990).

The UVic ESCM employs a vertically integrated energy-moisture balance atmospheric model for computational efficiency, the underlying philosophy being that on time scales greater than a decade the ocean is a key prognostic component of the climate system (Weaver 2004). Momentum conservation equations are replaced by specified wind fields and the thermodynamic energy balance equations are vertically integrated. This leaves a single atmospheric layer that captures the climatic mean state in the absence of atmospheric variability. Radiative forcing associated with changes in atmospheric CO_2 is included as a change in the outgoing longwave radiation. Precipitation in the form of rain or snow occurs when the relative humidity exceeds 85%. Surface winds are prescribed from a longterm monthly mean climatology.

Precipitation on land is treated by a simple bucket model, detailed by Matthews et al. (2003). Inputs to the bucket are rain and snowmelt; outputs are evaporation and river runoff. Runoff occurs when a grid cell's 15 cm deep bucket overflows, and it is returned instantaneously to the ocean via weighted river discharge points. The parameterization of evaporation on land includes a surface resistance. Surface resistance decreases as a bucket

fills and is dependent on vegetation type calculated by a land-surface and vegetation model.

The sea ice model incorporates energy conserving ice-snow thermodynamics with a 2-category thickness distribution (Bitz et al. 2001), and an elastic-viscous-plastic rheology (Hunke and Dukowicz 1997). The model predicts ice thickness, areal fraction and surface temperature.

The UVic ESCM has been used to investigate many scientific questions in both contemporary and paleoclimates. The model was validated against present-day climatology in Weaver et al. (2001) and various proxy paleo-reconstructions in Schmittner et al. (2002), Meissner et al. (2003) and Cottet-Puinel et al. (2004). Its computational efficiency and ability to maintain a stable climate without explicit flux adjustments permits a wide range of parameter sensitivity studies over long timescales (e.g. Wiebe and Weaver (1999), Lewis et al. (2003), Ewen et al. (2004)).

2.1.2 Current study

As described in Section 1.3.2, projections of future atmospheric CO_2 levels vary widely depending on various societal and physical parameters (Houghton et al. 2001). Two sets of experiments are conducted in which atmospheric CO_2 is altered over time (Figure 2.1). The first uses prescribed equilibrium-CO_2 profiles that bracket the range of stabilization scenarios suggested by the IPCC Special Report on Emission Scenarios (Nakićenović et al. 2000). The second involves atmospheric CO_2 pulses based roughly on the modelling results of Ewen et al. (2004) and Archer and Buffett (2005).

In all model integrations, atmospheric CO_2 increases from 1850 preindustrial levels (280 ppmv) following the exponential profile of Weaver et al. (2000), based on the two-parameter exponential fit of the observed 1850-1990 increase in atmospheric CO_2 and other gases used by Mitchell et al. (1995):

$$C_t = C_{PI} e^{(a(t-1850)^b)} \tag{2.1}$$

where C_{PI} = 280 ppmv, a = 7.944 x 10^{-8}, b = 3.0058 and t is the time in years. In the equilibrium-CO_2 experiments, CO_2 is capped at years 2000, 2050 and 2100 and then held constant. In the pulsed-CO_2 experiments, CO_2 is capped at year 2000, 2050 and 2100 levels and then is decreased over 2000 years to 20% of the original exponential increase. This simulates drawdown of atmospheric CO_2 during ocean/atmosphere equilibration. A final run increases CO_2 to year 2100 then decreases it over 500 years to 20% of the original exponential increase. All model runs are integrated for 3000 years or more to allow for ocean thermal equilibration.

2.2 The GHSZ model

The GHSZ model utilizes a 1-D thermal diffusive model and a methane hydrate three-phase equilibrium curve to determine depth to the BHSZ and is forced by model-derived temperature changes at the seafloor and prescribed sea level rise.

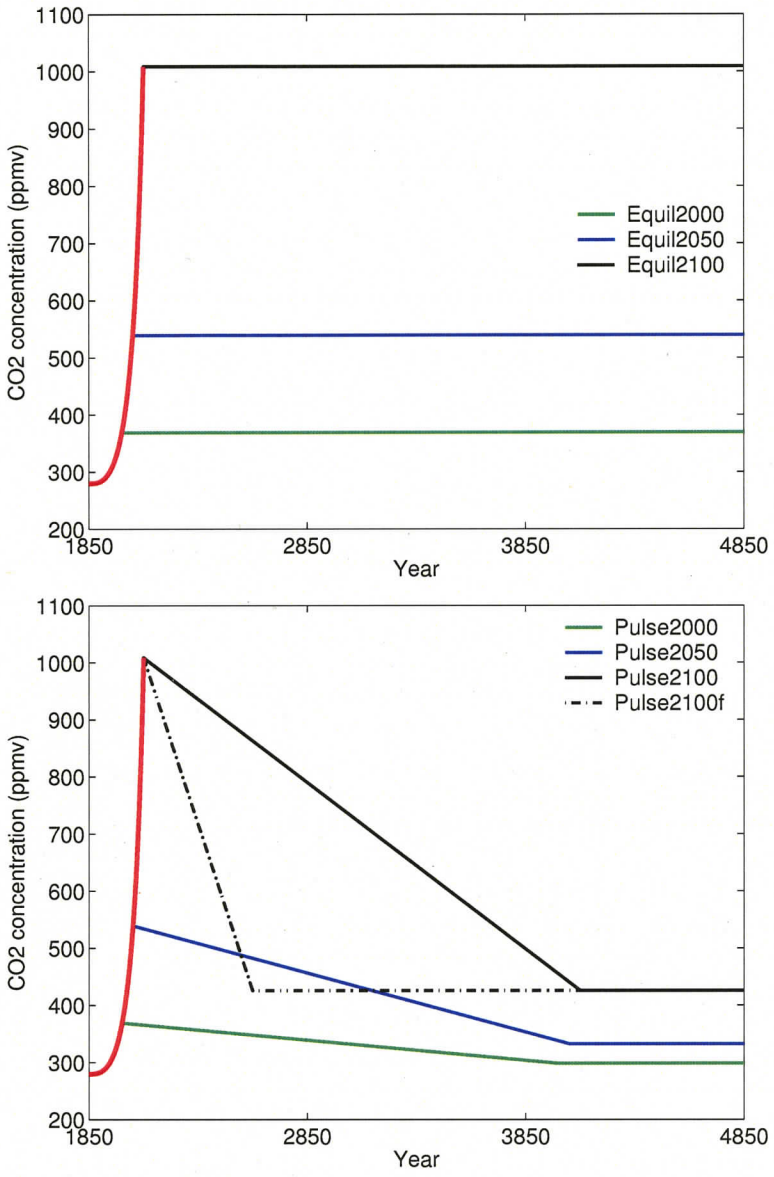

Figure 2.1: CO_2 profiles used to force the UVic ESCM. The upper panel details the equilibrium-CO_2 experiments and the lower details the pulsed-CO_2 experiments.

2.2.1 1-D thermal diffusive model

The approach of Xu et al. (2001) is followed in constructing the sediment thermal diffusion model to determine the time-and-depth-dependent temperature $T(t, z)$. Heat transfer within the modeled seafloor is assumed to occur solely due to vertical diffusion of heat. An initial linear temperature-depth profile ($T(0, z)$) is specified:

$$T(0, z) = T(0, 0) + Gz \tag{2.2}$$

where G is the geothermal gradient and $T(0,0)$ corresponds to the preindustrial seafloor temperature at each grid cell. Perturbations to this initial state are based on subsequent climate model temperature output which is applied to the thermal diffusion equation:

$$\frac{\partial T}{\partial t} = \kappa \frac{\partial^2 T}{\partial z^2} \tag{2.3}$$

where κ = effective thermal diffusivity. If it is assumed that the geothermal gradient at infinite depth remains constant, the solution of equation 2.3 is:

$$T(t,z) = T(0,z) - \frac{z}{2\sqrt{\pi\kappa}} \int_0^t T([t-x],0) x^{-\frac{3}{2}} e^{-\frac{z^2}{4\kappa x}} dx - T(0,0)\mathrm{erfc}(\frac{z}{2\sqrt{\kappa t}}) \tag{2.4}$$

Equation 2.4 is solved iteratively to model geothermal evolution at each GHSZ model grid point (Figure 2.2).

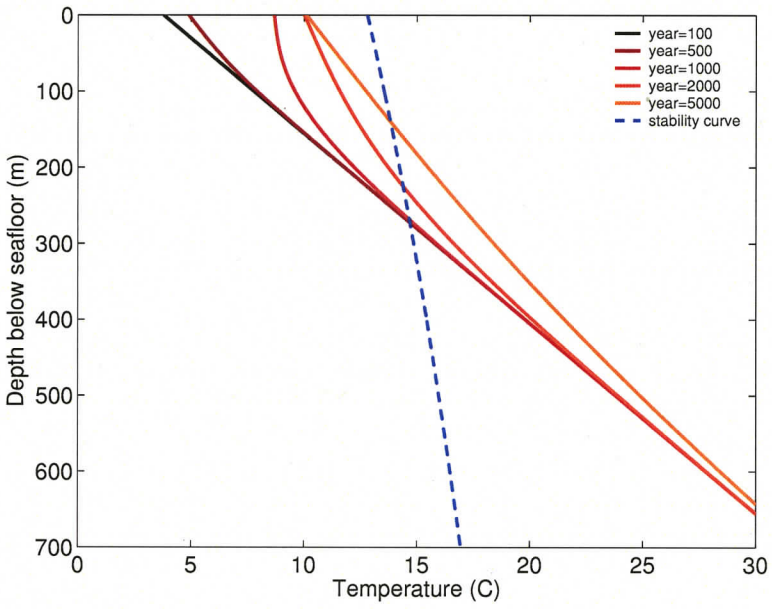

Figure 2.2: Typical evolution of the thermal diffusive model over time in response to a warming seafloor. The blue dashed line represents the methane hydrate equilibrium curve.

Fourier's law states that the geothermal gradient obeys:

$$G = q/k \tag{2.5}$$

(where k = bulk thermal conductivity (W/mK) and q = heat flow (W/m^2). Both heat flow and thermal conductivity can vary significantly over the seafloor. The average heat flow from the ocean floor calculated by Pollack et al. (1993) is 101 mW m^{-2}. However, heat flow along continental margins is significantly lower than this average due primarily to a colder lithosphere. For example, Harvey and Huang (1995) use an average geothermal heat

flow of 70.3 mW m^{-2} over their prescribed methane hydrate reservoir. Heat flow also varies along-margin as a function of margin type (passive or active). Bulk thermal conductivity depends on sediment and material within the pore space which itself varies significantly as a percentage of the total volume. Water or hydrate have lower conductivities (~0.6 and ~0.5 W/mK respectively) than the rock matrix (~1.7-6.1 W/mK, Turcotte and Schubert (1982)). Due to the various factors affecting the regional variation of the geothermal gradient and in the interest of simplicity, calculation of the initial geothermal gradient is avoided and is instead prescribed: values of 0.04°C/m and 0.06°C/m are used. In this manner, the response of a range of realistic GHSZ volumes to climate change can be studied. An initial linear geotherm assumes that the seafloor is at thermal equilibrium prior to the prescribed CO_2 increase. This is likely a valid first-order assumption given the relative stability of the Holocene climate of the last 10 kyr (Petit et al. 1999). Additionally, pressure effects within the seafloor associated with a lower sealevel during the last glacial maximum are not likely to have persisted to the present day, particularly if pressure within the shallow seafloor is able to respond instantaneously to pressure at the seafloor/ocean interface.

Thermal diffusivity is calculated as:

$$\kappa = \frac{k}{\rho c} \tag{2.6}$$

(k = bulk thermal conductivity, ρ = bulk density and c = specific heat). As thermal diffusivity can vary widely both vertically and horizontally depending on sediment/rock type, bulk density and pore space/content, a single calculated diffusivity is avoided and a range of thermal diffusivities spanning plausible realistic values (similar to the approach used for the geothermal gradient) are used: κ = 1 x $10^{-7}m^2/s$, 5 x $10^{-7}m^2/s$ and 10 x $10^{-7}m^2/s$. As the value of thermal diffusivity strongly affects the response time of the marine GHSZ to seafloor temperature changes, the use of a range of diffusivity values brackets realistic response times of the GHSZ to potential future climate change.

2.2.2 Methane hydrate three-phase equilibrium curve

The gas hydrate three-phase equilibrium curve describes the line in P-T space where hydrate, gas and liquid coexist. As described in Section 1.2.1, this curve depends on a number of factors including composition of the source gas, composition of the pore waters, and sediment type and structure. Dickens and Quinby-Hunt (1994) examined the stability of methane hydrate in a seawater solution for pressures ranging from 3-10 MPa, and Brown et al. (1996) fit a second-order polynomial to this data for extrapolation to greater depths:

$$T(z) = 11.726 + 20.5\log_{10}z - 2.2(\log_{10}z)^2 \tag{2.7}$$

where z is the depth below the seafloor (km) and T(z) is the temperature at which the three phase equilibrium curve is reached (Figure 2.3).

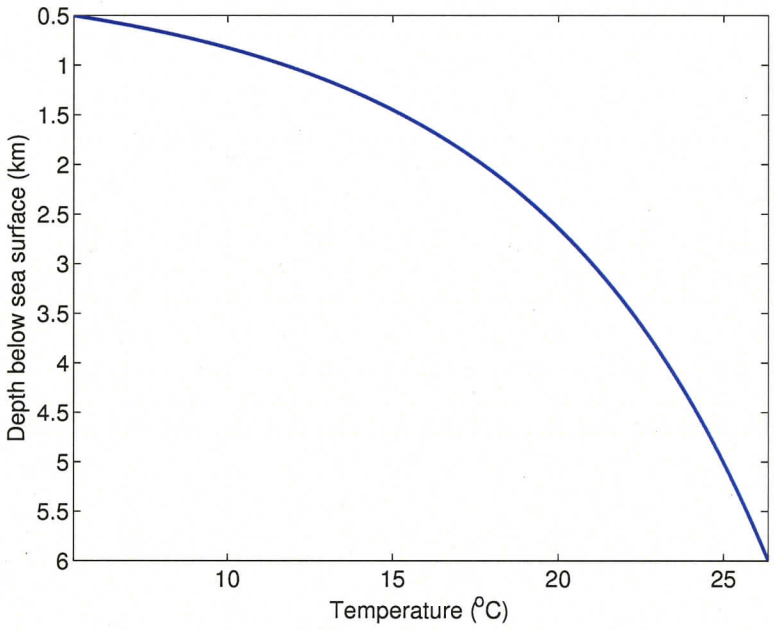

Figure 2.3: 3-phase equilibrium curve as a function of temperature.

This curve-fit is used based on the comparison of various fits to the data of Dickens and Quinby-Hunt (1994) carried out by Peltzer and Brewer (2000) and is the formulation used within the GHSZ model to predict the three phase equilibrium curve as a function of depth.

Section 1.2.1 described the factors that shift the three phase equilibrium curve in P-T space. The formulation of the equilibrium curve adopted here assumes that the marine gas hydrate reservoir is filled with pure methane gas that occupies all voids in the hydrate lattice. This produces a minimum BHSZ depth, as the addition of even small fractions of different molecular species increases the range of the stability field. The surrounding pore water is assumed to be identical to sea water in composition. A fresher (less briny) porewater would increase the stability field; this has been suggested as a negative feedback to hydrate dissociation due to the release of fresh water into the pore space during melting. At steady state, however, the composition of the pore water is thought to be similar to seawater, and any anomalous pore water chemistry is eventually flushed out of the system by the diffusion of seawater into the sediments.

2.2.3 Determination of the BHSZ

The intersection of the equilibrium curve (Equation 2.7) with the temperature-depth profile (Equation 2.4) marks the bottom of the GHSZ. Below this point, despite increasing pressure, the temperature will always be too high for methane hydrates to form. A Newton-Raphson procedure is used to identify this intersection to < 1 cm accuracy. Typically 4-6 iterations are needed to locate this intersection when searching from below plausible BHSZ depths. A caveat of this method is that zones of instability that occur immediately below the seafloor

(the 'Case 1' scenario of Harvey and Huang (1995)) are not detected, as this second intersection always occurs at shallower depths within the sediment column. However, thermally equilibrated sediment columns of this sort are uncommon and the exclusion of these upper unstable zones affects the global GHSZ volume negligibly (Harvey and Huang 1995). If no intersection is detected within 10 iterations or the intersection occurs above the seafloor depth, the BHSZ for that location and time is set to 0 m.

2.2.4 Horizontal GHSZ extent

While simplistic, the approach of determining the horizontal extent of the GHSZ region largely captures the regions determined by more sophisticated methods. A weakness in using present-day seafloor carbon concentrations or sea surface chlorophyll measurements to propose regions of increased hydrate accumulations (e.g. Gornitz and Fung (1994), Harvey and Huang (1995)) arises due to the asymmetry of timescales between hydrate buildup ($\sim 10^6$ years) and variations in upwelling sites ($\sim 10^3$ years). Potential variations in upwelling regions in response to changing oceanographic conditions have likely shifted upwelling sites significantly on timescales shorter than that of hydrate accumulation, such that present-day regions of organic carbon deposition may not necessarily correspond to at-depth increases in carbon content. An explicit calculation of seafloor organic carbon content within the model as a function of depth is not feasible due to the idealized bathymetry of the UVic ESCM. However, increased carbon rain, sedimentation and upwards fluid flow has always occurred more along continental margins than the open ocean, and it is this limiting factor that is used in the present study. In order to better constrain distance from land, GHSZ model cells are calculated at 3x the resolution of that of the climate model. In such a configuration, the GHSZ model resolution is 1.2°x0.6° and defines a horizontal GHSZ that extends uniformly ~133 km from all coastlines (Figure 2.4). This distance-from-shore is of the same order of magnitude as the typical average continental margin width (including shelf and slope) of ~200 km quoted by Kennett (2003) and 100 km used in the GHSZ calculations of Dickens (2001).

However, it is essential to note that the GHSZ model is still constrained by the resolution of input from the climate model (3.6°x1.8°); the increase in GHSZ resolution is only carried out to create a better representation of horizontal GHSZ extent. In particular, bathymetry is passed from the UVic ESCM directly to the GHSZ model. This potentially introduces a 'deep' bias to depths used by the GHSZ relative to higher-bathymetry datasets which more accurately represent shallow continental shelves and margins. This occurs particularly at low latitudes where the UVic ESCM exhibits the lowest horizontal resolution (one degree of longitude = 111 km at the equator but 0 km at the poles). However, the use of these high-resolution data sets is avoided in order to preserve internal consistency between model-derived seafloor depths and seafloor temperatures. Had one used ETOPO-5, a 5'x5' bathymetric dataset, shallow bathymetry would consistently overlie deep-water temperatures and/or ETOPO-5 continents with model ocean, resulting in erroneous calculations

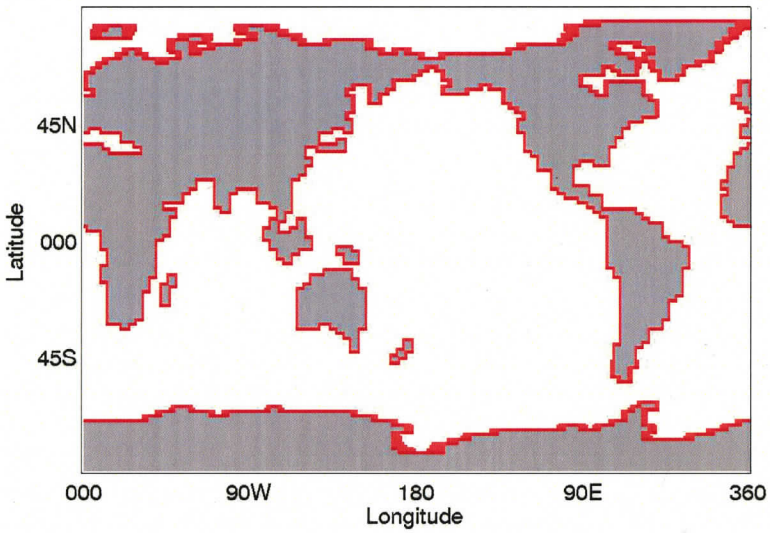

Figure 2.4: Horizontal extent (in red) of the GHSZ used in GHSZ model construction.

of the BHSZ. The idealized nature of the model bathymetry must be accepted in order to model climate change over thousands of years using an intermediate complexity model such as the UVic ESCM, with the obvious caveat that the absolute magnitude of the global GHSZ volume depends on the idealized nature of the climate model.

2.2.5 Hydrate distribution

The distribution of hydrate within the sediment is a function of porosity and hydrate occupancy of that porosity. As the current model does not include equations of fluid flow or mass transfer (it is purely thermodynamic) hydrate is prescribed as a function of depth. This approach allows for first-order approximations of the mass of methane stored in the global GHSZ, but does not truly predict the distribution of hydrate as predicted by mechanistic models such as that of Xu and Ruppel (1999). Additionally, this prescribed hydrate does not interact with the thermal diffusive model through latent heat effects (see Section 2.2.6). The sediment porosity profile used here decreases exponentially from 60% at the seafloor with an e-folding depth of 1.5 km (Davis and Hyndman 1990). Hydrate is prescribed to fill 5% of the available porosity at the BHSZ, with occupancy decreasing linearly to 1% of available pore space at the seafloor; this assumes that the GHSZ is everywhere saturated with respect to methane and combines the fluid-flow and in-situ end-member formation cases of Gornitz and Fung (1994). A linear increase/decrease in the prescribed hydrate occupancy or GHSZ extent would result in a corresponding increase/decrease in the mass of methane due to the prescribed nature of the hydrate occupancy within the GHSZ, and so represents an arbitrarily tuneable aspect of the model configuration.

2.2.6 Latent heat and dissociation-induced pressure change

As the hydrate distribution within the sediment is simply prescribed (i.e. it is not an interactive component of the model), the latent heat of melting involved in the endothermic melting of methane hydrates is not taken into account in the thermal diffusive model. During hydrate formation/dissociation heat is produced/absorbed. This process potentially slows the rate of propagation of heat into the sediment and is proportional to the percent volume of hydrate. Xu et al. (2001) suggest that over long timescales ($\sim 10^4$ years) this process is negligible. Bangs et al. (2005) and Mienert et al. (2005) use formulations of heat diffusion that neglect latent heat effects when modelling changes in the hydrate stability zone. Both authors indicate, however, that the exclusion of latent heat from their formulations results in the 'fastest' case of migration of the BHSZ for a given thermal diffusivity; this constraint also applies to the results presented here.

The dissociation of methane hydrates results in gas production, potentially leading to volume expansion and/or overpressuring in the absence of gas escape (either through diffusion or concentrated flow along pre-existing or induced fracture paths). The results presented here assume that gas is allowed to escape from the BHSZ at a rate greater than that of gas production due to dissociation. This assumption results in an absence of pressure-induced stabilization of gas hydrates.

The effect of important approximations used in the GHSZ model are summarized in Table 2.1.

Approximation	**Effect on GHSZ model results**
Constant κ, G	Ignores regional and vertical variation of seafloor thermal properties
κ	Underestimates/overestimates GHSZ response time to thermal perturbations if too high/low
G	Underestimates/overestimates BHSZ depths if too high/low
Pore-water salinity	Underestimates/overestimates BHSZ depths if too saline/fresh
Pure methane hydrate	Underestimates BHSZ depths
Horizontal GHSZ extent	Underestimates/overestimates GHSZ size and response time if too small/large
UVic ESCM bathymetry	Regionally overestimates or underestimates GHSZ volume and response time to thermal perturbations
Hydrate occupancy of GHSZ	Underestimates/overestimates carbon within GHSZ if too low/high
No latent heat effects	Underestimates GHSZ response time to external perturbations
No pressure effects	Underestimates GHSZ response time to external perturbations

Table 2.1: Approximations used in the construction of the GHSZ model, and their effect on model results.

2.3 ESCM-GHSZ Model coupling

Bathymetry and 100-year averaged time-mean seafloor temperature fields (the seafloor temperature is taken to be equal to the temperature of the deepest ocean grid cell) are obtained from the UVic ESCM for the first 3000-4000 years (i.e. the duration of the climate model integrations) and applied to the GHSZ model using 100 year timesteps. Seafloor temperatures for the remaining GHSZ model integrations are assumed to be equal to the last output from the UVic ESCM. This is justified as the UVic ESCM for all model integrations is integrated until the ocean mean temperature equilibrates and no further change to deep sea temperatures is expected. Long GHSZ model timesteps are justified due to the slow diffusion of heat into the sediments and the relatively slow rate of change of seafloor temperature.

Chapter 3

Modelling Results

3.1 Initial conditions

The simulated preindustrial steady state seafloor temperature is shown in Figure 3.1. The global average preindustrial seafloor temperature is 1.9°C and the average seafloor temperature over the prescribed continental margin is 4.3°C. The simulated preindustrial steady

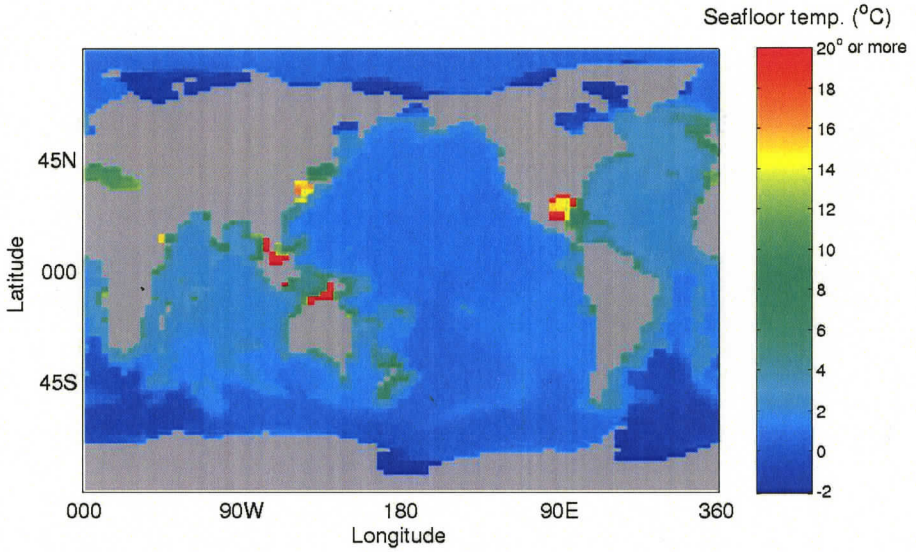

Figure 3.1: Preindustrial steady state seafloor temperature.

state GHSZ exists along continental margins and is shown by Figure 3.2. Depths to the BHSZ vary as a function of bathymetry, model-derived seafloor temperature and prescribed geothermal gradient. Maximum BHSZ depths occur along deep, cold continental margins and extend to more than 600 m below the seafloor (mbsf). Several areas of the continental margin exhibit a total lack of GHSZ due to warm seafloor temperatures and/or shallow depths, notably the Gulf of Mexico, Weddell Sea, Timor Sea and Hudsons Bay. Methane hydrate is known to occur extensively in the Gulf of Mexico (Milkov and Sassen 2000), and the lack of modelled methane hydrate there reflects the coarse bathymetry used in the UVic ESCM which limits depths within the Gulf of Mexico to no greater than 500 m.

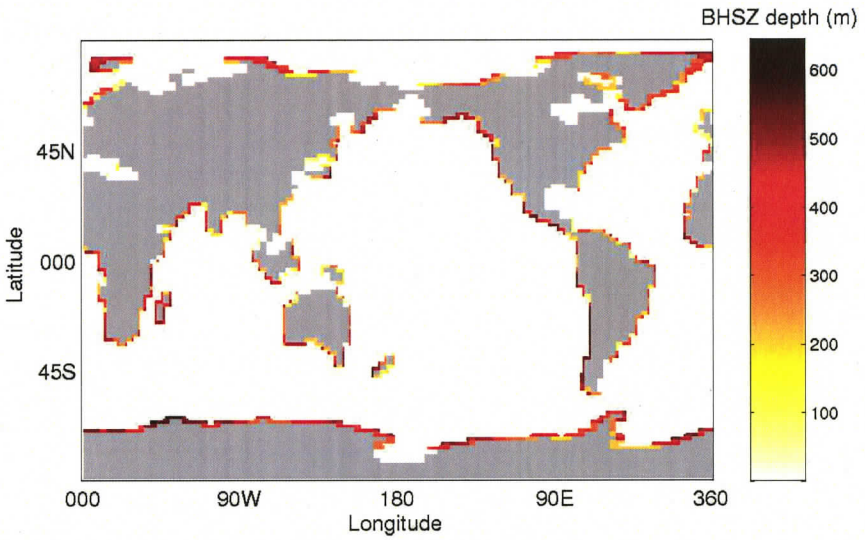

Figure 3.2: The global pre-warming GHSZ, G=40°C/km. The depth to the BHSZ varies with seafloor depth and seafloor temperature. Note areas that exhibit a lack of GHSZ due to shallow model bathymetry and/or warm seafloor temperatures.

As explained in Section 2.2.4, the application of modelled seafloor temperatures to a high-resolution topography is avoided in the interest of global model consistency, resulting in this regional model/observation conflict. Volumes of the global GHSZ (using parameterizations given in Section 2.2) for the preindustrial model state are given in Table 3.1. These values are comparable to other published estimates (Milkov 2004). The GHSZ contains 6500 Gt C if $G = 0.04$ °C/km and 4400 Gt C if $G = 0.06$ °C/km, when using the hydrate-filling scheme outlined in Section 2.2.5. While the purpose of this work was not to develop a new estimate of the global inventory of hydrate-bound methane, it is important that the approach lead to reasonable global values since it is the first-order response of these values to global climate change that is of primary interest.

	GHSZ volume (km^3)
Present study, $G = 0.04$	$6.7x10^6$
Present study, $G = 0.06$	$4.3x10^6$
Milkov (2004)	$7x10^6$
Harvey and Huang (1995)	$16.5x10^6$
Gornitz and Fung (1994)	$5\text{-}13.9x10^6$

Table 3.1: Preindustrial global GHSZ volumes (using $G = 0.04$°C/m and 0.06°C/m) compared to other estimates.

3.2 Equilibrium CO_2 experiments

Three equilibrium CO_2 experiments (Equil2000, Equil2050 and Equil2100, see Figure 2.1) were carried out to assess the maximum possible response of the GHSZ to climate change.

In each experiment CO_2 increased exponentially (Equation 2.1 and Figure 2.1) and was then held constant until seafloor thermal equilibration occurred.

3.2.1 UVic ESCM results

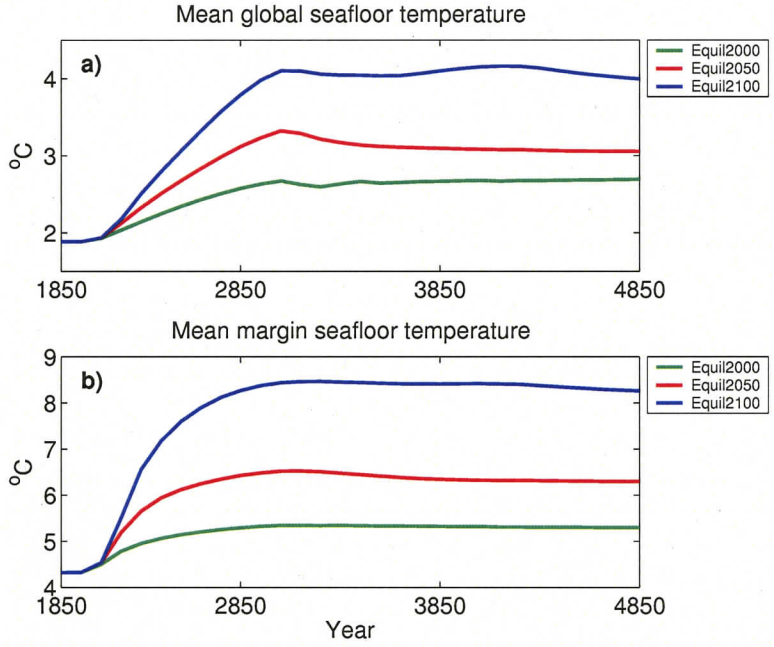

Figure 3.3: Evolution of seafloor temperatures during equilibrium CO_2 integrations. A) Global average seafloor temperature evolution; B) average margin temperature evolution.

Maximum seafloor warming from initial preindustrial values lags the CO_2 increase by several hundred years due to the time taken for thermal diffusion and water mass convection and advection to transport heat into the ocean interior. Global average seafloor temperature increases by 0.8°C for Equil2000, 1.2°C for Equil2050 and 2.1°C for Equil2100 (Figure 3.3a). However, seafloor temperature increases exhibit large spatial variability, with the presence of significantly greater warming along continental margins (Figure 3.4). The average temperature increases there by 1.0°C for Equil2000, 2.0°C for Equil2050 and 3.9°C for Equil2100 (Figure 3.3b). For comparison, global average surface air temperature increases by 1.7°C for Equil2000, 3.8°C for Equil2050 and 6.9°C for Equil2100.

Major regional spatial variability in seafloor temperature change is primarily the result of bathymetry: shallower regions of the seafloor warm more (Figure 3.5). Additional spatial variability arises due to two additional processes: the strength and location of vertical water advection (primarily high latitude deep water formation and wind-driven downwelling) and sea ice extent.

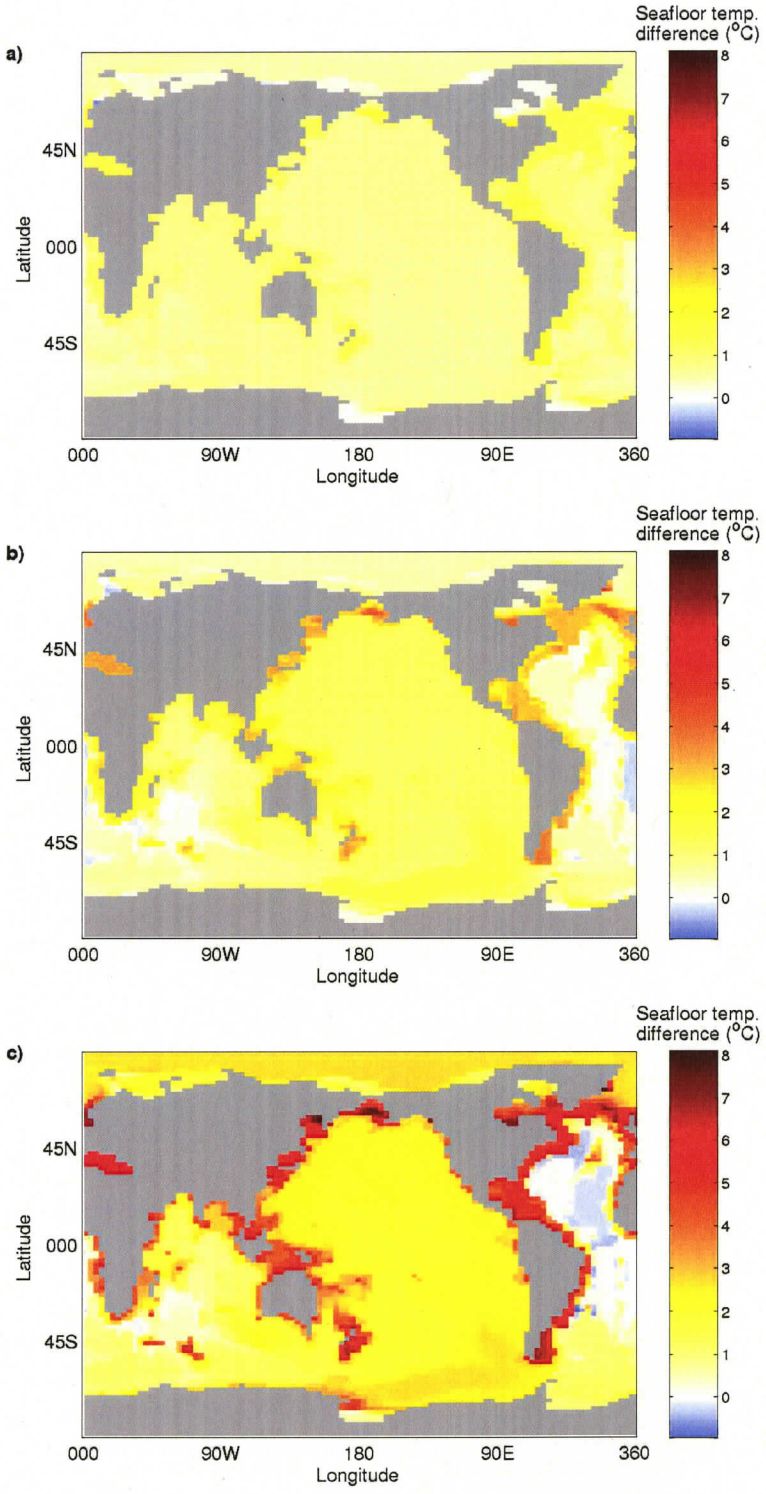

Figure 3.4: (Equilibrium - preindustrial) seafloor temperature differences. A) Equil2000; B) Equil2050; C) Equil2100. Note the larger temperature increase along continental margins and decreases in the Atlantic seafloor temperature in Equil2050 and Equil2100.

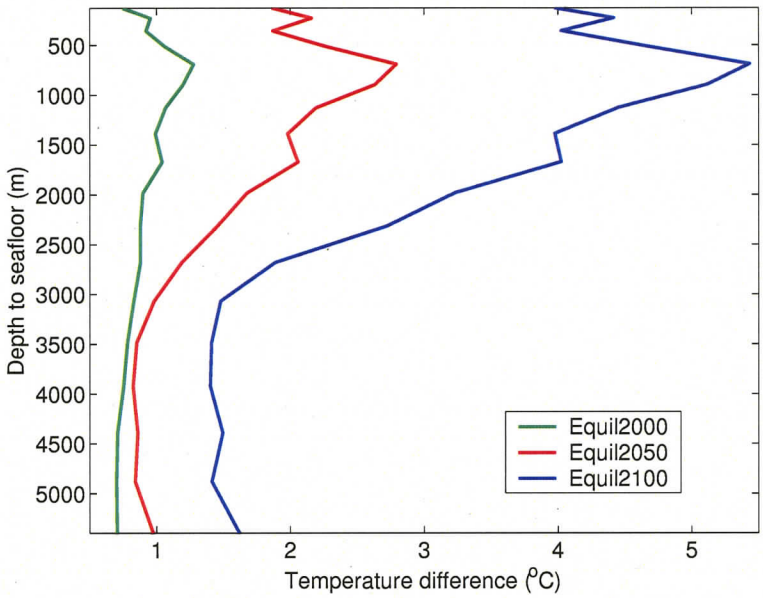

Figure 3.5: (Equilibrium - preindustrial) seafloor temperature differences as a function of depth. The magnitude of seafloor warming generally decreases with depth except for a prominent subsurface maxima in seafloor warming at 800 mbsf.

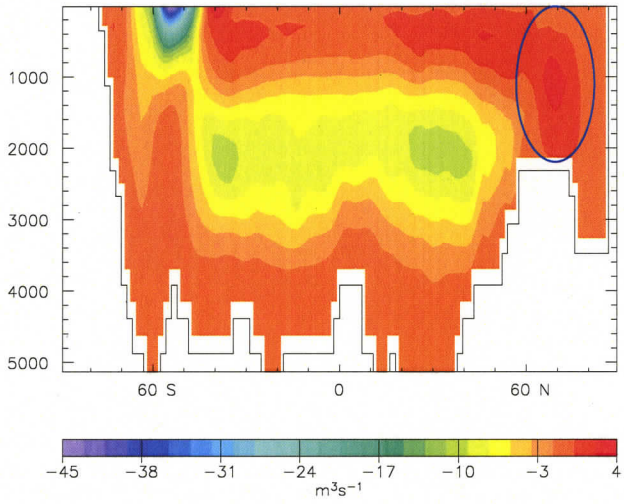

Figure 3.6: (Equilibrium - preindustrial) Atlantic meridional overturning streamfunction difference, Equil2100. Increased downwelling as a result of northward movement of the NADW circulation cell is indicated by the blue circle. Shallowing of the NADW cell results in the decrease in intermediate-depth northward transport.

Vertical water advection

The strength of North Atlantic meridional overturning in all runs initially decreases in response to rising CO_2 then returns to equal or higher post-warming equilibrium values, consistent with the earlier work of Weaver (2004). The site of deep water formation migrates

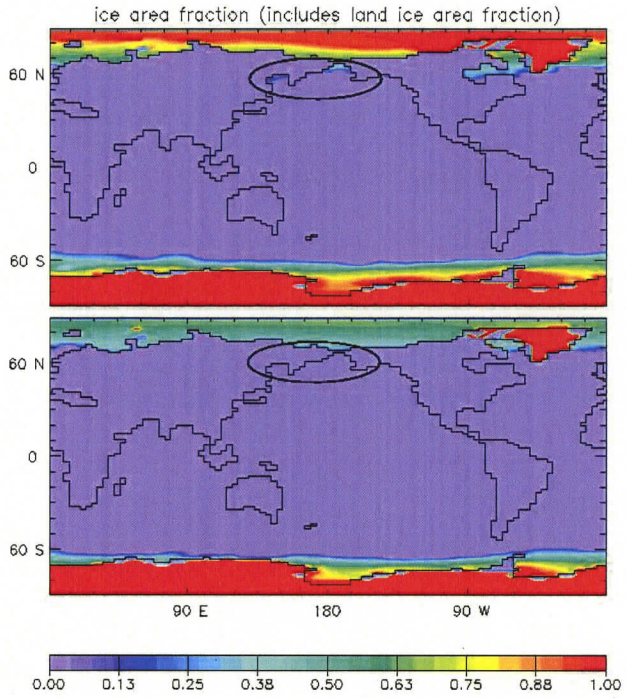

Figure 3.7: Percentage ice coverage, Equil2100. A) year 1850; B) year 2250. Note the poleward retreat of sea ice edge in both hemispheres and the loss of sea ice in the Barents and Okhotsk Seas (circled).

northeast in Equil2050 and Equil2100 in response to a retreating sea ice edge (Figure 3.6). This results in the sudden delivery of warm, saline NADW water to a region of the Greenland Sea that was previously covered by colder Arctic bottom water. This region therefore experiences a large seafloor temperature increase (Figure 3.4b/c).

The NADW cell also shallows significantly (Figure 3.6) with the magnitude of shallowing dependent on the CO_2 scenario. This leads to a counter-intuitive seafloor temperature change in Equil2050 and Equil2100 as a strengthened AABW (Figure 3.6) invades the North Atlantic, decreasing temperatures there by up to 1°C. This has implications for paleoclimate inferences from deep-sea sediment cores: a high-CO_2 environment characterized by warm surface temperatures may be reflected in the deep Atlantic by *cooler* abyssal temperatures.

Variation in downwelling as a result of Eckman pumping may also play a role in regulating temperatures along continental margin seafloors. As the winds in the UVic ESCM do not vary interannually, variation in the amount of downwelling can only arise in the model due to changes in the stability of the density-stratified water column. As surface waters typically warms more than intermediate or deep waters (Figure 3.5), the depth of Eckman pumping will likely decrease, thereby counteracting to some extent the warming of continental margins by reducing the transport of warm surface water to depth. However, this effect was not quantitatively isolated during model integrations.

Sea ice

As sea ice melts, darker ocean water is uncovered and the local albedo decreases, resulting in greater absorption of incoming radiation. This increases the rate of warming which drives more sea ice loss in a positive feedback loop. High latitude, shallow margins that experience this "sea-ice/albedo feedback effect" (Figure 3.7) correspond to regions that exhibit large regional seafloor temperature increases. Of particular note are the Okhotsk and Bering Seas which display the largest seafloor warming in the model domain. The Antarctic continental margin also loses a large percentage of perennial sea ice cover but because of deep marginal bathymetry the large surface warming signal does not reach the seafloor.

3.2.2 GHSZ model results

The global GHSZ response to the atmospheric CO_2 increase is delayed due to the time required for heat to be transported through the water column and then diffused into the seafloor to the BHSZ. The heterogeneity of the spatial GHSZ response reflects the rates and magnitudes of regional seafloor temperature changes, as well as bathymetry, and therefore varies significantly along continental margins (Figure 3.8). The absolute magnitude and response of the global GHSZ volume for all equilibrium-CO_2 experiments is summarized graphically in Figure 3.9. As seafloor temperature change is a function of atmospheric CO_2 increase (Section 3.2.1), the global GHSZ volume decreases the least for Equil2000 and the most for Equil2100. A steeper geothermal gradient results in shallower BHSZs, a smaller absolute GHSZ volume and a quicker response to thermal perturbations at the seafloor. Higher thermal diffusivity results in a quicker response to seafloor temperature change as heat is diffused rapidly to the BHSZ. For experiments with $\kappa = 10 \text{ x } 10^{-7}$ m^2/s, the majority of the GHSZ response to increasing ocean temperatures occurs within 5000 years of the initiation of the atmospheric CO_2 increase, whereas experiments with $\kappa = 1 \text{ x } 10^{-7}$ m^2/s are still experiencing GHSZ adjustment after 40 kyr.

Important regions are those in which the BHSZ shoals to the seafloor in response to increased seafloor temperatures, rendering the entire column unstable with respect to methane hydrate. In these regions, methane that is mobilized during hydrate dissociation is not able to re-form higher up in the sediment column and is therefore most likely to enter the exogenic carbon cycle. Cells within the model domain that experience total GHSZ loss are therefore binned during each model run, and the spatial and temporal distribution of these cells are examined to give an indication of areas and times that are potentially most prone to large-scale methane flux into the ocean or atmosphere.

Using κ=5 x 10^{-7} m^2/s, Equil2000 experiences some regions with total GHSZ loss, particularly in locations within the Okhotsk Sea and off the coast of Britain (Figure 3.10a). These cells, totalling approximately 1% of the total continental margin area, occur in regions of shallow bathymetry that exhibit shallow pre-warming BHSZs (maximum 88 mbsf). The first cells to experience total GHSZ loss appear after 400 years of model integration (year

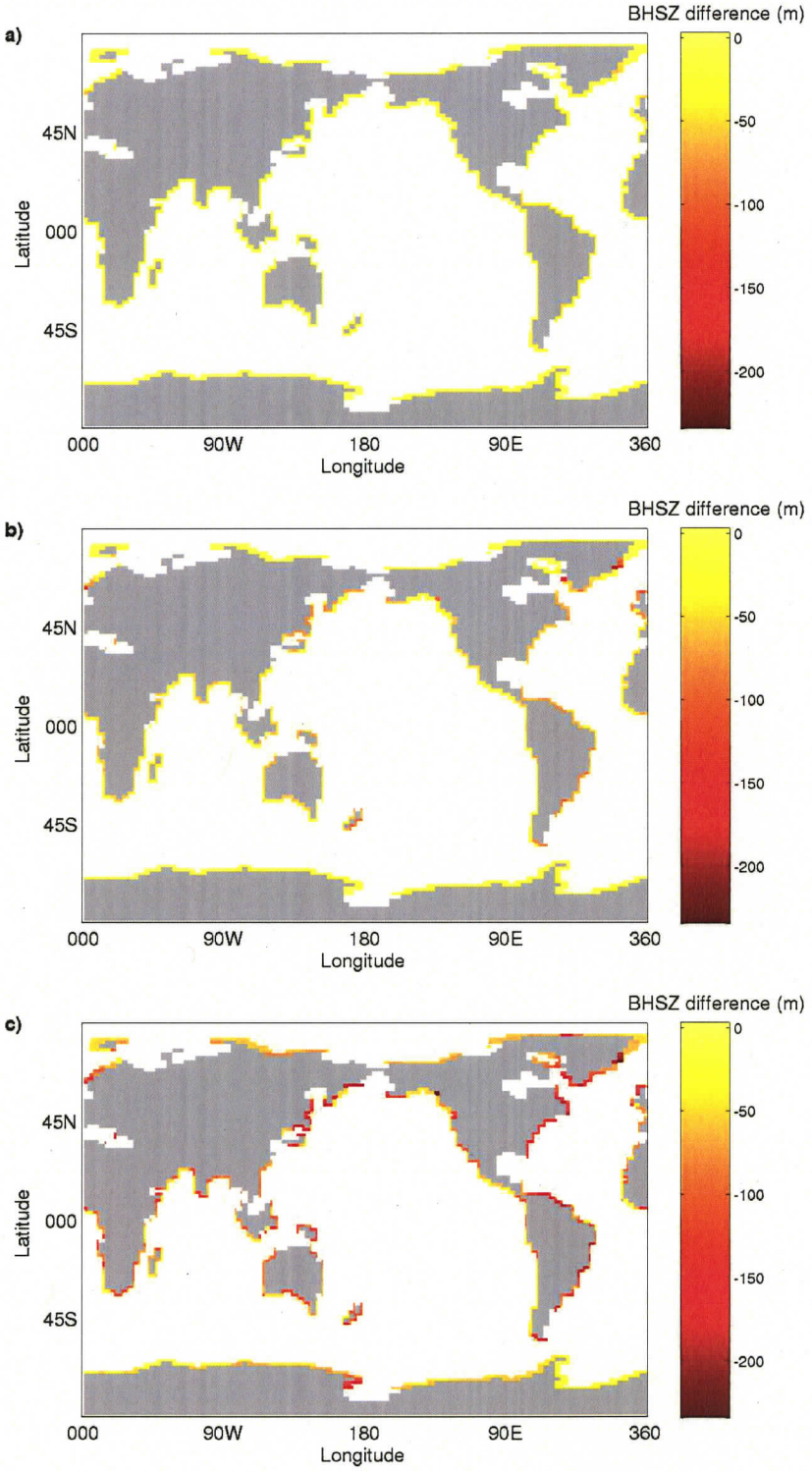

Figure 3.8: 40 kyr - preindustrial BHSZ depth difference, G = 40°C/km, κ = 1 x 10^{-7} m^2/s. A) Equil2000; B) Equil2050; C) Equil2100.

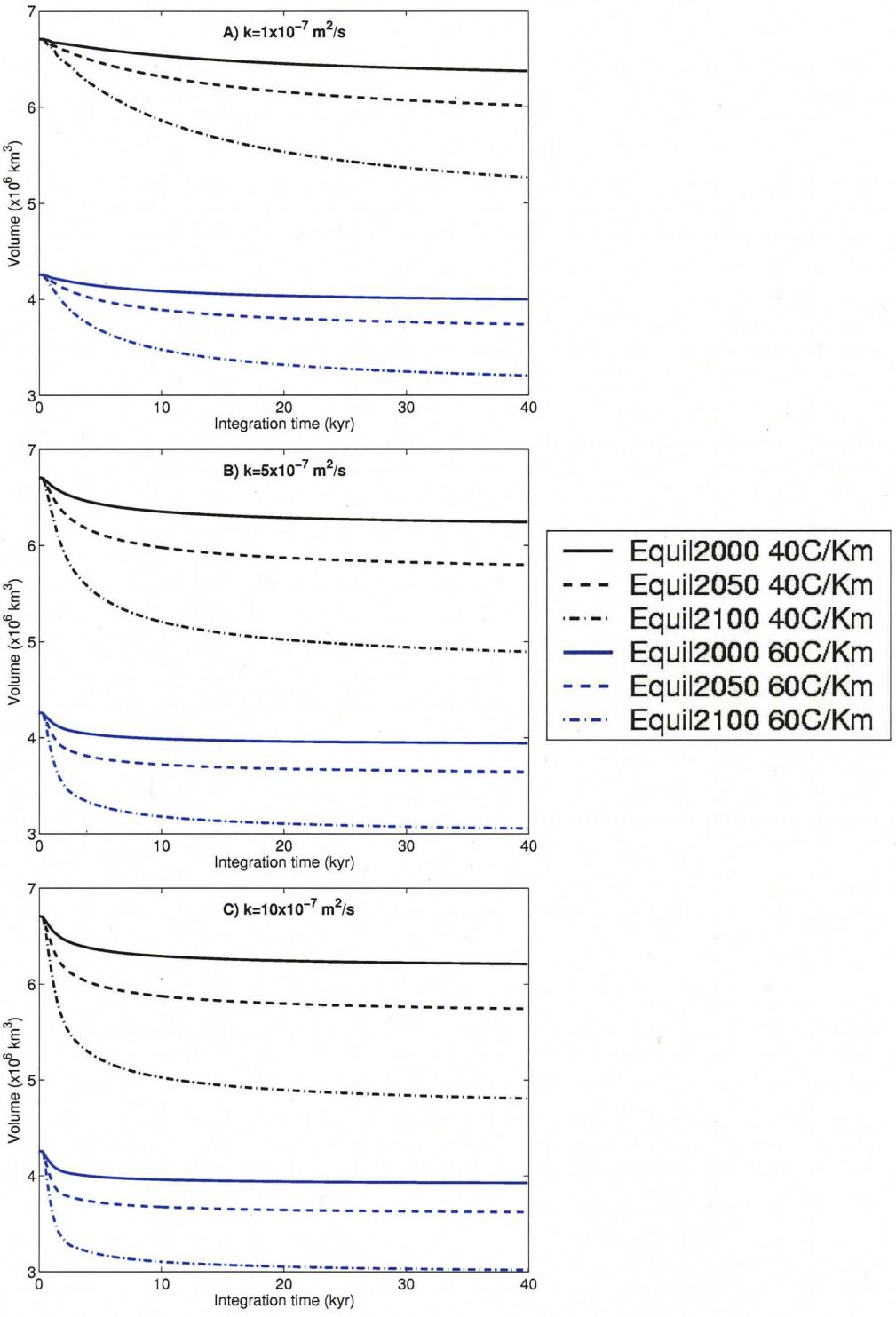

Figure 3.9: Evolution of the global GHSZ volume under equilibrium-CO_2 forcing using varying values of geothermal gradient and thermal diffusivity.

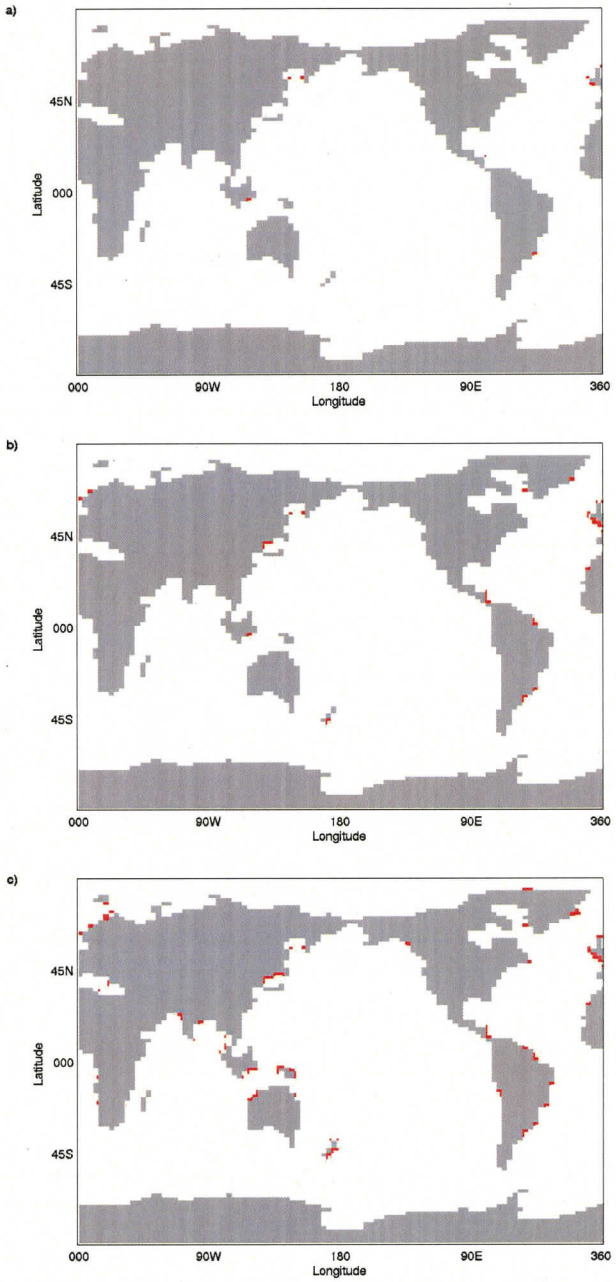

Figure 3.10: Regions that experience total GHSZ loss after 40 kyr (G = 40°C/km), κ = 5 x 10^{-7} m^2/s): a) Equil2000; b) Equil2050; c) Equil2100. Red denotes areas where the BHSZ has shallowed to the seafloor.

2250), and subsequent cells become completely unstable with respect to methane hydrate for the next 900 years (until year 3150).

Equil2050 exhibits a greater area under which complete GHSZ loss occurs with binned cells appearing over 4% of the total margin area (Figure 3.10b), including coherent regions

around Britain, New Zealand and in the Japan Sea. GHSZs are totally destabilized from depths of up to 190 mbsf over a period beginning 400 years into the model integration and lasting for 2300 years.

Equil2100 displays the greatest amount of total GHSZ loss, with 9% of the continental margin (Figure 3.10c) completely destabilizing from depths of up to 239 mbsl. Regions of coherent total GHSZ loss that existed in Equil2050 increase in size and numerous additional regions appear along continental margins. The period over which cells experience total GHSZ loss in Equil2100 begins 400 years into the model integration and lasts for 2900 years.

Higher/lower values of thermal diffusivity will lead to faster/slower development of 100% loss regions but because the GHSZ model is forced by a permanently warmer ocean (as a result of holding CO_2 fixed) the absolute magnitudes of GHSZ lost and carbon mobilized for different diffusivity values will eventually converge, given the same seafloor temperature forcing.

Decreases in the GHSZ volume after 40 kyr, total carbon mobilized through dissociation, areal extent of 100% GHSZ loss regions and the mass of carbon mobilized in these regions, for all equilibrium-CO_2 scenarios, are given in Table 3.2.

	Equil2000			**Equil2050**			**Equil2100**		
ΔT_G (°C)	**0.8**			**1.2**			**2.1**		
ΔT_M (°C)	**1.0**			**2.0**			**3.9**		
κ (x10^{-7} m^2/s)	*1*	*5*	*10*	*1*	*5*	*10*	*1*	*5*	*10*
40C/km									
ΔV_{max} (%)	5	7	7	10	14	14	21	27	28
ΔM_{tot} (Gt C)	312	422	450	646	833	879	1360	1688	1764
ΔA_{100} (%)	1	1	1	3	4	4	8	9	9
ΔM_{100} (Gt C)	14	14	14	81	89	89	290	307	319
60C/km									
ΔV_{max} (%)	6	7	8	12	14	14	25	28	29
ΔM_{tot} (Gt C)	262	315	327	520	607	627	1061	1204	1237
ΔA_{100} (%)	1	1	1	4	4	4	9	9	9
ΔM_{100} (Gt C)	8	8	8	52	52	52	186	195	195

Table 3.2: GHSZ response to equilibrium CO_2 experiments. ΔT_G = maximum average global seafloor temperature increase; ΔT_M = maximum average margin seafloor temperature increase; ΔV_{max} = maximum global GHSZ volume decrease expressed as a percent loss of the initial GHSZ volume; ΔM_{tot} = total C mobilized during GHSZ loss; ΔA_{100} = percent of margin area experiencing 100% GHSZ loss; ΔM_{100} = C mobilized from 100% GHSZ loss regions.

3.3 Pulsed CO_2 experiments

A range of experiments was carried out in which atmospheric CO_2 was first increased then relaxed to lower levels. Such experiments are meant to explore the response of the global GHSZ to CO_2 profiles similar to those presented in the studies of Ewen et al. (2004) and

Archer and Buffett (2005) in which global carbon cycle feedbacks are taken into account. Specific CO_2 forcing profiles are detailed in Figure 2.1. In particular, three runs were carried out in which CO_2 was increased exponentially to years 2000, 2050 and 2100 then decreased linearly over 2000 years to 20% of the initial rise. These experiments are termed Pulse2000, Pulse2050 and Pulse2100, respectively. An additional run was carried out in which CO_2 was allowed to increase exponentially to year 2100, then decrease over only 500 years to levels equal to 20% of the original rise. The purpose of this experiment, termed Pulse2100f, is to explore the effects of different rates of CO_2 decrease on the global GHSZ.

3.3.1 ESCM model results

The global average seafloor temperature in all pulsed-CO_2 experiments experiences an initial temperature increase which then relaxes to new a equilibrium determined by the atmospheric CO_2 stabilization concentration (Figure 3.11a). The global average seafloor

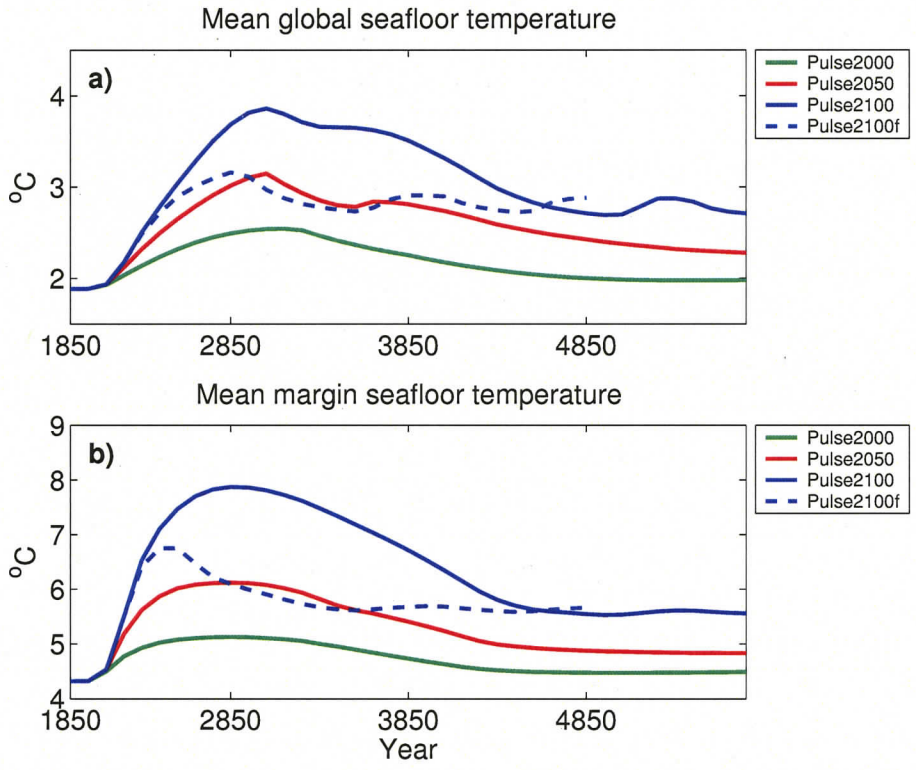

Figure 3.11: Evolution of seafloor temperatures during pulsed-CO_2 experiments. A) Global average seafloor temperature evolution; B) average margin temperature evolution. Note that all runs except for Pulse2100f were run for an additional 800 years to reach equilibrium.

temperature peak lags the CO_2 peak by approximately 700 years and the adjustment to a new steady state occurs over a period of approximately 2000 years, during which the atmospheric CO_2 also gradually decreases and is then held steady. As with the equilibrium

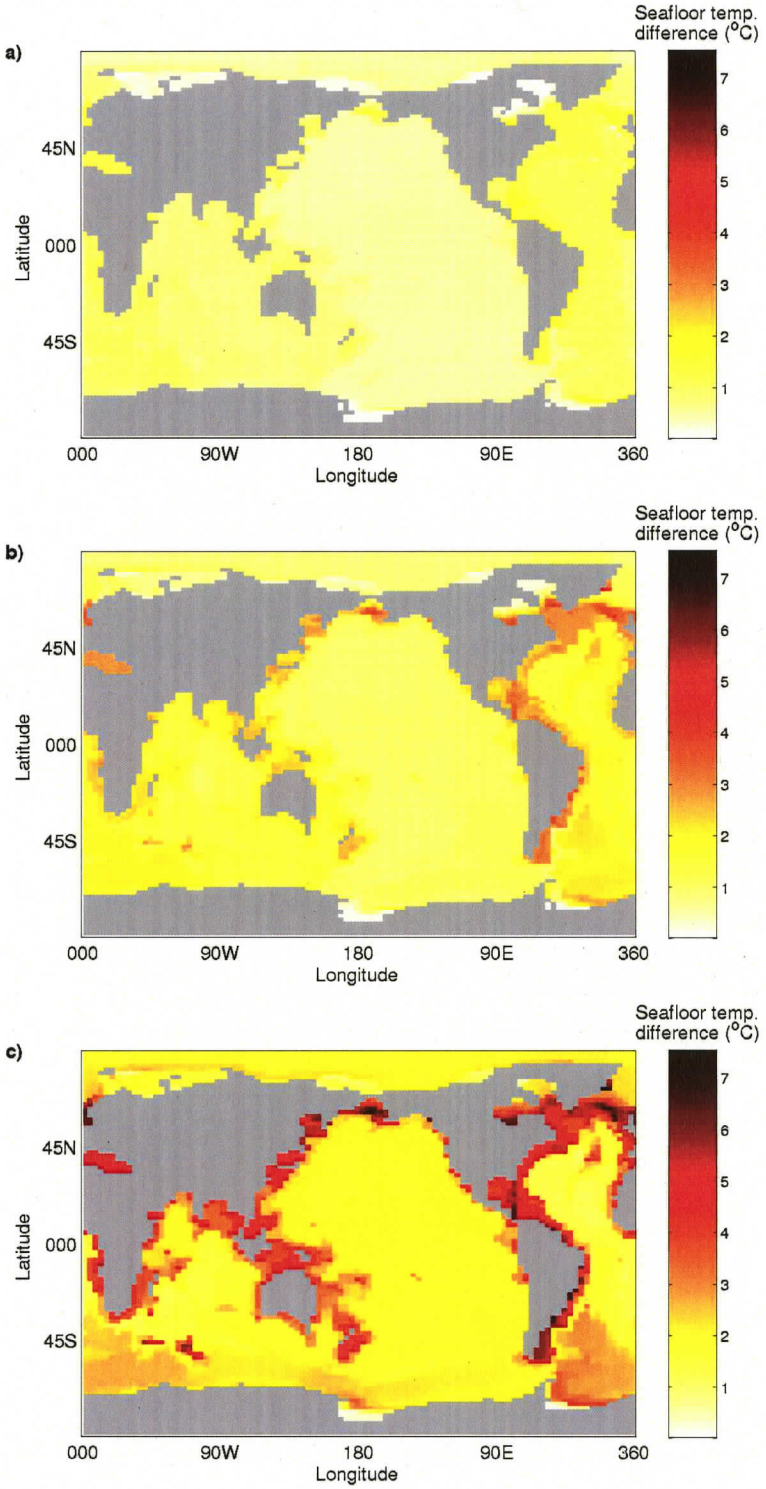

Figure 3.12: Maximum seafloor temperature increases for pulsed-CO_2 experiments. A) Pulse2000; B) Pulse2050; C) Pulse2100.

CO_2 model integrations, the continental margin seafloor temperature typically increases more than the global average and equilibrates slightly sooner (Figure 3.11b). Figure 3.12 illustrates the maximum seafloor warming experienced by each of the pulsed-CO_2 scenarios. Maximum temperatures are slightly less than those achieved by equilibrium CO_2 runs.

3.3.2 GHSZ model results

GHSZ model integrations forced by pulsed-CO_2 experiments typically exhibit an initial decrease in the global GHSZ volume followed by a gradual equilibration to levels determined by final seafloor temperatures. The absolute magnitude and response of the global GHSZ volume for all pulsed-CO_2 experiments is summarized graphically in Figure 3.13. The evolution of the global GHSZ depends largely on the difference between the thermal timescale (Equation 1.1) at average BHSZ depths (237 m for preindustrial conditions with $G = 0.04°C/m$ and 150 m for preindustrial conditions with $G = 0.06°C/m$) and the length of the thermal pulse produced by the transient CO_2 forcing. Factors that affect the thermal timescale are (in decreasing order of importance) thermal diffusivity, length of the thermal pulse (related to the length of the atmospheric CO_2 pulse) and geothermal gradient.

For low κ, the thermal timescale is more than the length of the thermal pulse, resulting in a smoother transition between pre- and post-pulse GHSZ states. As the value of thermal diffusivity increases, the thermal perturbation penetrates deeper into the seafloor, resulting in a greater pulsed response of the global GHSZ volume. In particular, the response of the GHSZ varies significantly between runs with $\kappa = 1x10^{-7}$ m^2/s and $\kappa = 5x10^{-7}$ m^2/s, suggesting that future predictions of marine methane hydrate response to climate change require accurate κ values.

Comparison of Pulse2100 and Pulse2100f integrations (Figure 3.14) shows the effect of altering the rate of CO_2 decrease on the GHSZ volume. A gradual CO_2 decrease (Pulse2100) results in a longer thermal pulse to the seafloor and a greater response of the GHSZ while a rapid CO_2 pulse (Pulse2100f) results in a negligible initial response from the GHSZ.

As the geothermal gradient increases, the distance to the BHSZ (analogous to the thermal skindepth D in Equation 1.1) shallows and a greater temperature increase occurs there. This effect, coupled with a small initial absolute GHSZ volume, result in a large relative response of the GHSZ to high-geothermal gradient integrations (Table 3.3.

The spatial extent of 100% GHSZ loss regions in pulsed-CO_2 experiments is only slightly affected by variation of κ and geothermal gradient. The percentage of the prescribed continental margin that experiences 100% GHSZ loss (ΔA_{100}) is slightly less than runs forced with equilibrium CO_2 levels. In all runs except those with $\kappa = 1x10^{-7}$ m^2/s, all cells that exhibit 100% loss do so during the initial GHSZ decrease period (i.e. before year 3350); as the GHSZ recovers to post-pulse levels no further 100% GHSZ loss regions occur. In runs with $\kappa = 1x10^{-7}$ m^2/s, the thermal pulse is not 'seen' at typical BHSZ depths and most 100% GHSZ loss occurs in response to post-pulse equilibrium seafloor temperatures. This results in a marked decrease in ΔA_{100} for low-κ integrations. Finally, a doubling of

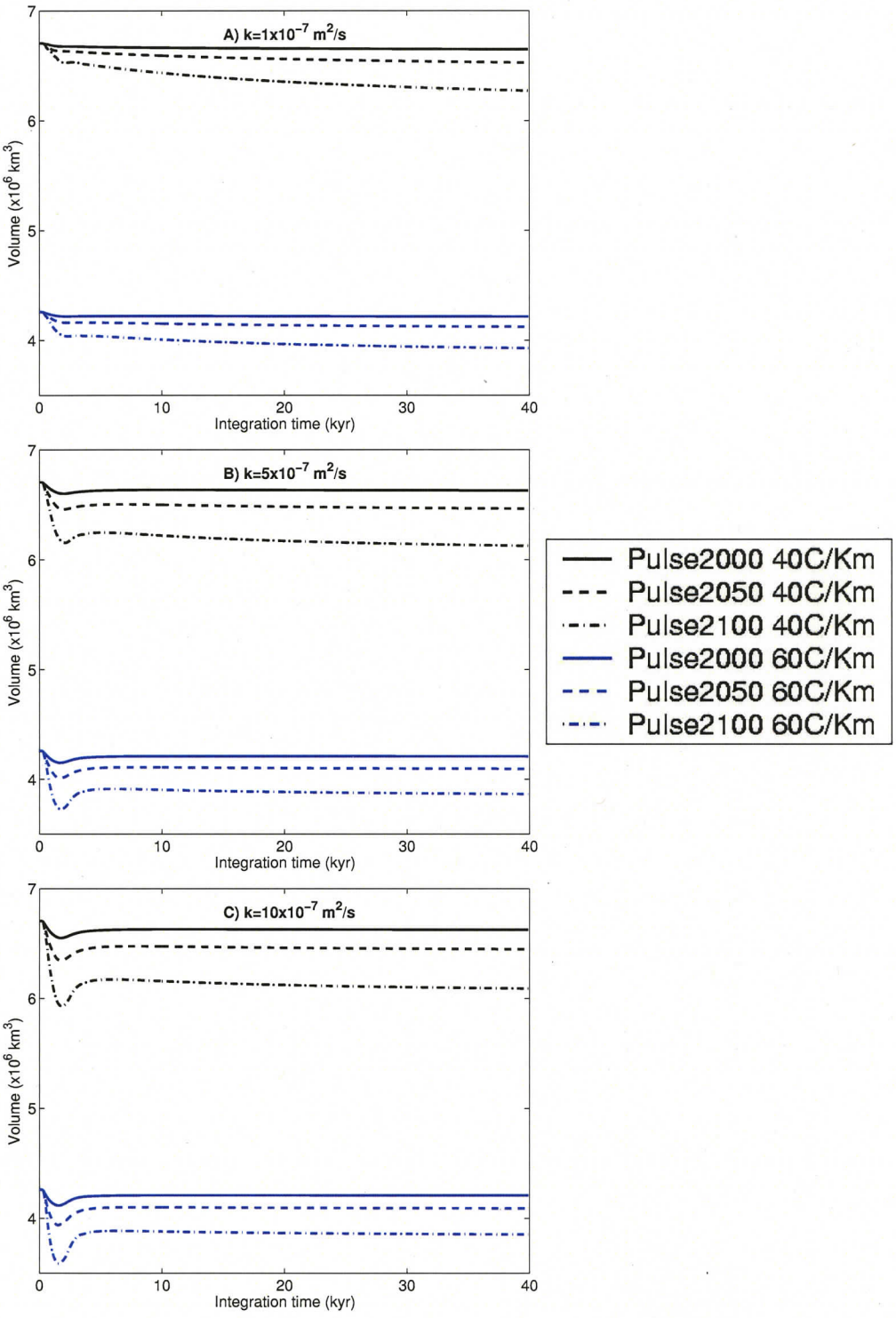

Figure 3.13: Evolution of the global GHSZ volume under pulsed-CO_2 forcing using varying values of geothermal gradient and thermal diffusivity. Note the initial pulsed decrease in the global GHSZ volume in response to pulsed temperature perturbations at the seafloor.

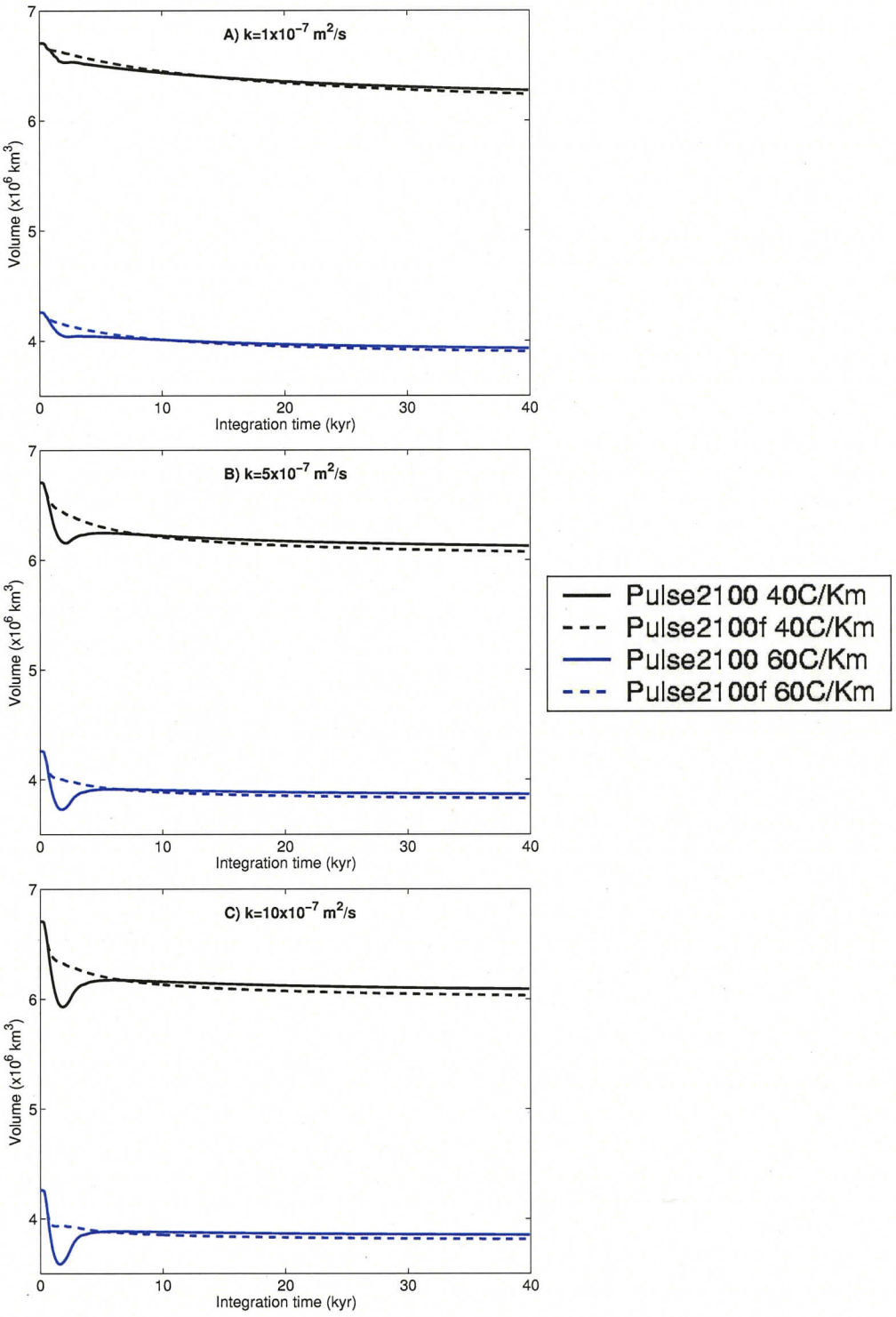

Figure 3.14: Comparison of GHSZ response to Pulse2100/Pulse2100f forcing. Due to the smaller temperature pulse at the seafloor, the GHSZ volume under Pulse2100f forcing experiences a negligible initial decrease compared to the prominent decrease exhibited by integrations forced by Pulse2100.

the areal extent of 100% GHSZ loss for Pulse2100 compared to Pulse2100f reflects the sustained seafloor warming that occurs for a gradual decline of atmospheric CO_2 versus a rapid decrease (Figure 3.11).

It is important to note that the presence of significant hydrate deposits would affect the evolution of the global GHSZ volume in pulsed-CO_2 experiments through the stabilizing effect of dissociation-induced latent cooling. As the GHSZ model does not include parameterization of latent heat effects, the initial pulsed decreases in the GHSZ volume presented here represent the maximum rate of response of the GHSZ reservoir: any hydrates occurring at the BHSZ will effectively reduce the BHSZ migration rate and decrease the magnitude of the pulsed response (roughly analagous to the effect of decreasing κ).

Table 3.3 details the maximum change in GHSZ volume after 40 kyr, total carbon as methane mobilized through the dissociation of hydrates, areal extent of 100% GHSZ loss regions and the mass of carbon mobilized in these regions, for all pulsed-CO_2 scenarios.

	Pulse2000			**Pulse2050**			**Pulse2100**			**Pulse2100f**		
ΔT_G (°C)	**0.7**			**1.3**			**2.0**			**1.3**		
ΔT_M (°C)	**0.8**			**1.8**			**3.6**			**2.4**		
κ (x10^{-7} m^2/s)	*1*	*5*	*10*	*1*	*5*	*10*	*1*	*5*	*10*	*1*	*5*	*10*
40C/km												
ΔV_{max} (%)	1	2	2	3	4	5	6	9	12	7	10	10
ΔM_{tot} (Gt C)	72	135	179	210	341	423	477	751	901	445	618	671
ΔA_{100} (%)	1	1	1	3	3	3	5	8	8	3	4	4
ΔM_{100} (Gt C)	4	4	4	55	66	70	147	254	254	54	93	101
60C/km												
ΔV_{max} (%)	1	3	3	3	6	8	8	12	16	8	10	11
ΔM_{tot} (Gt C)	69	130	164	187	304	369	418	643	759	372	469	512
ΔA_{100} (%)	1	1	1	3	3	3	7	8	8	3	4	4
ΔM_{100} (Gt C)	2	2	2	39	39	41	124	156	156	44	60	60

Table 3.3: GHSZ response to pulsed CO_2 experiments after 40 kyr. ΔT_G = maximum mean global seafloor temperature increase; ΔT_M = maximum mean margin seafloor temperature increase; ΔV_{max} = maximum global GHSZ volume decrease expressed as a percent loss of the initial GHSZ volume; ΔM_{tot} = total C mobilized during GHSZ loss; ΔA_{100} = percent of margin area experiencing 100% GHSZ loss; ΔM_{100} = C mobilized from 100% GHSZ loss regions.

3.4 Atmospheric feedback experiments

The escape of carbon from thermally dissociated methane hydrates into the exogenic carbon cycle provides a potential positive thermal feedback mechanism to the Earth system. If hydrate-derived carbon is able to enter the atmosphere, the radiative effects of both the original CH_4 and oxidized carbon CO_2 will drive further warming. As the atmospheric lifetime of CH_4 is short (~10-12 years) and the carbon is applied to the UVic ESCM in pulses, it is practical to consider only the radiative effects of the end-member CO_2, because the radiative impact of each CH_4 addition will decay exponentially on the order of the

methane atmospheric lifetime which is short compared to the length of time between pulses of CH_4.

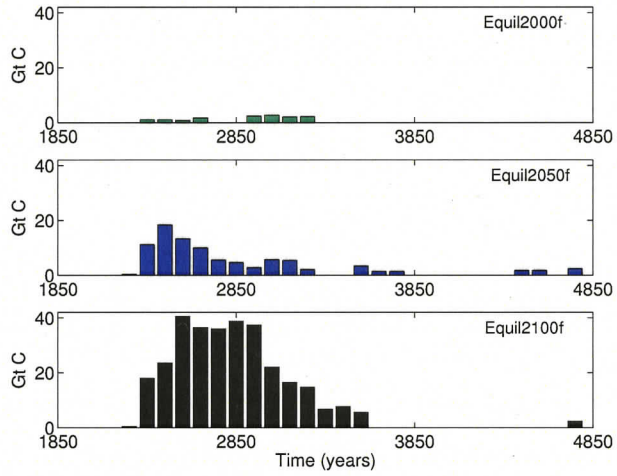

Figure 3.15: Magnitude and timing of carbon additions to the UVic ESCM resulting from 100% GHSZ loss regions. Note that discrete pulses, not gradual fluxes, were added to the UVic ESCM.

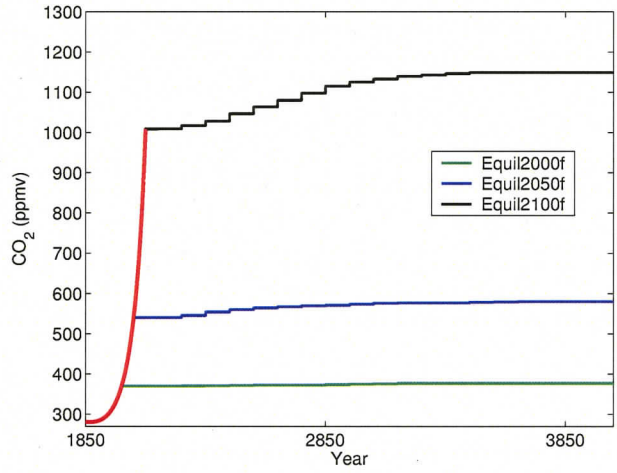

Figure 3.16: CO_2 profiles resulting from addition of hydrate-derived carbon to the model atmosphere. The stepwise increase in CO_2 after the initial exponential increase results from the addition of carbon as CO_2 from GHSZ model cells that experience total GHSZ loss. Each stepwise increase therefore reflects the instantaneous addition of carbon from all the model cells that undergo 100% GHSZ loss within that timestep of the GHSZ model.

To simulate the potential feedback of hydrate-source carbon on the climate system, CH_4 from GHSZ model cells experiencing total GHSZ loss during equilibrium-CO_2 runs (κ = 5x10^{-7} m^2/s and G = 0.04°C/m) is converted to CO_2 and added instantaneously to the atmosphere as soon as soon as total GHSZ loss at each cell occurs (Figure 3.15). This

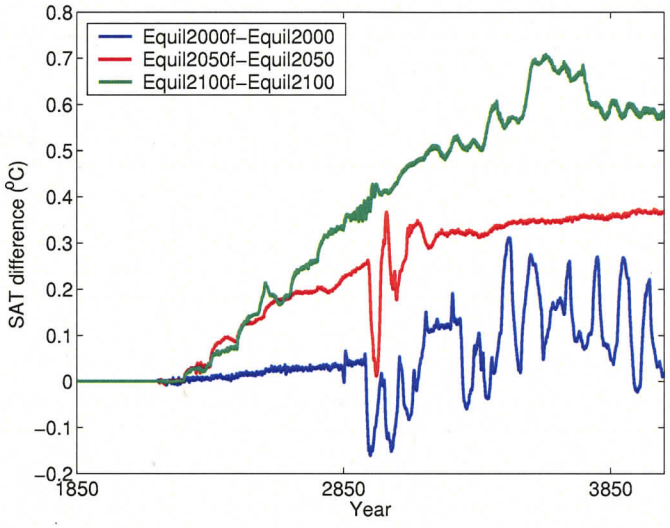

Figure 3.17: SAT temperature differences between equilibrium-CO_2 integrations with prescribed CO_2 and both prescribed + hydrate-derived CO_2 forcing. Large periodic oscillations in SAT are likely caused by rapid adjustments in the sea-ice extent that are not mirrored by the other model run of the comparison.

assumes that the ocean does not oxidize any outgoing CH_4, and results in a series of pulsed additions of CO_2 to the atmosphere.

If a cell does not experience complete GHSZ loss during the integration, no carbon is added from that cell to the atmosphere; this assumes that any methane mobilized in such situations re-forms as hydrate in the shallowed GHSZ. The hydrate-derived CO_2 (Figure 3.16) is added to the prescribed CO_2 levels; a comparison surface air temperatures (SAT) of these runs with original 'no-feedback' runs allows an estimate of the feedback factor of the marine methane hydrate reservoir. Climate model runs incorporating hydrate-derived carbon are termed Equil2000f, Equil2050f and Equil2100f. Figure 3.17 shows the SAT difference between ESCM model integrations incorporating hydrate-derived atmospheric CO_2 and the original 'no-feedback' equilibrium-CO_2 integrations. After 2000 years, the SAT difference between Equil2000f and Equil2000 increases by less than 0.1°C. This difference increases to 0.4°C when comparing Equil2050 with Equil2050f, and 0.6°C when comparing Equil2100 with Equil2100f.

3.5 Steric sea level rise experiments

In order to determine the sensitivity of the GHSZ to potential increases in sea level due to the melting of continental ice sheets, hydrostatic pressure was adjusted over the first 1000 years of GHSZ model runs forced by equilibrium-CO_2 seafloor temperatures. Two idealized cases were considered: the melting of the GIS, and the melting of both the GIS and the WAIS. The former case was prescribed as a sea level increase of 6 m over 1000 years and the latter as an increase of 12 m over 1000 years.

Sea level rise buffers the effect of warming ocean temperatures so that decreases of the global GHSZ volume are in all cases less than no-sea-level-rise scenarios. However, this buffering effect is small during equilibrium CO_2 experiments (Figure 3.18) and decreases in relative magnitude as the magnitude of warming increases.

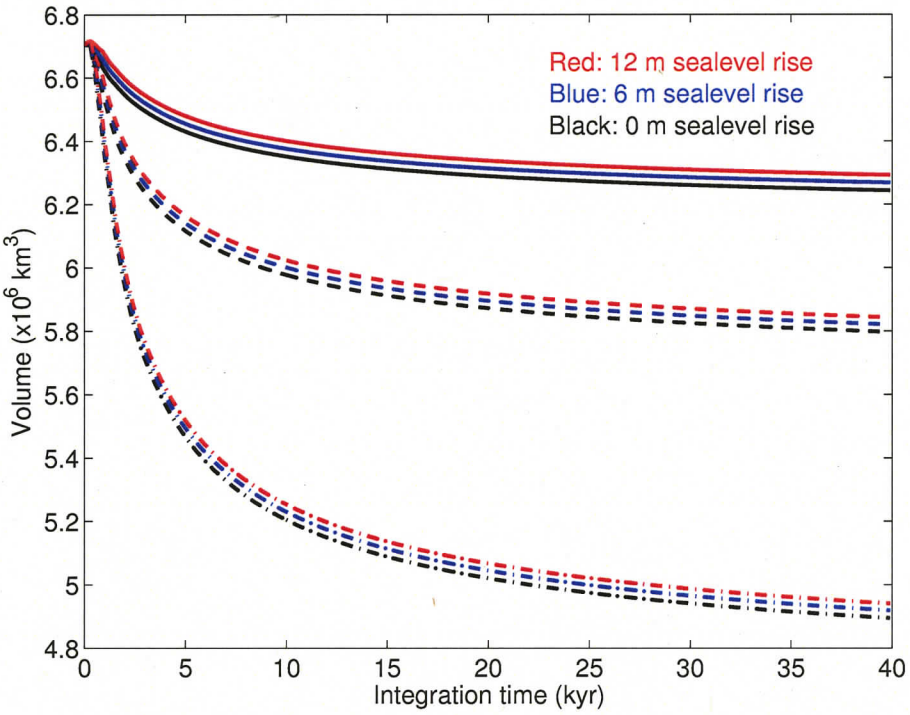

Figure 3.18: Effect of rising sea level on GHSZ volume evolution (40°C/km, $\kappa = 5\text{x}10^{-7}$ m^2/s). Solid curves: Equil2000; dashed curves: Equil2050; dot-dashed curves: Equil2100.

However, the stabilizing effect sea level rise is significant when binning cells that experience 100% GHSZ loss, particularly as the magnitude of seafloor warming decreases. With melting of both the GIS and WAIS, Equil2000 experiences a 40% decrease in margin area that experiences 100% GHSZ loss (compared to a no-sealevel-rise scenario), while the percentage decreases by 7% for Equil2050 and 3% for Equil2100. This reflects the sensitivity of the shallowest BHSZs to changes in temperature and pressure, because these cells make up a greater percentage of 100% GHSZ regions for experiments forced by lower CO_2 levels.

Chapter 4

Conclusions

The analysis presented here demonstrates the sensitivity of a simple marine methane hydrate stability model to potential future ocean warming. UVic ESCM integrations are forced with a range of CO_2 profiles corresponding to potential future climate scenarios, and the resulting seafloor temperatures are applied to a time-dependent 1-D GHSZ model. In this way, the response of the GHSZ to variations in seafloor temperature can be explored. Two sets of experiments are carried out. Equilibrium-CO_2 experiments are designed to gauge the maximum response of the GHSZ to equilibrium seafloor warming, while pulsed-CO_2 experiments provide insight into the response of the GHSZ to more realistic CO_2 forcing.

Seafloor warming caused by increases in atmospheric CO_2 exhibits large spatial variability, with the greatest warming occurring along continental margins. Additional variability arises from regional loss of sea ice and decreased albedo, and changes to the global thermohaline circulation system. The magnitude of global average seafloor warming is a function of both the maximum atmospheric CO_2 concentration and the time over which the CO_2 is held at that maximum level.

The response of the GHSZ to equilibrium-CO_2 experiments indicates that even for CO_2 concentrations held below present-day levels, the global GHSZ will decrease significantly due to warming ocean temperatures. After 40 kyr, the experiments carried out here indicate that the global GHSZ volume will shrink by between 5% and 29% in response to mean margin seafloor warming of between 1.0 and 3.9 °C. The rate and character of GHSZ decrease depends on the various CO_2 equilibrium levels and parameterizations of thermal diffusivity and geothermal gradient used in each experiment. Regions which exhibit 100% GHSZ loss represent sites where hydrate-bound carbon can most easily enter the exogenic carbon cycle, and range from 1% to 9% of the prescribed continental margin. If carbon from these regions is applied to the atmosphere in the form of CO_2, further warming of between <0.1-0.6°C results.

Pulsed-CO_2 experiments provide a demonstration of the interplay between rate of change in the temperature at the seafloor, seafloor thermal diffusivity and the GHSZ response. For quick thermal perturbations ($\sim 10^2$ years, Pulse_2100f) at the seafloor, or low thermal diffusivity ($\kappa < 5 \times 10^{-7}$ m^2/s), the thermal skin depth is shallower than the global average

BHSZ and the global GHSZ remains relatively unchanged. However, if a seafloor temperature perturbation persists for $\sim 10^3$ years or more (Pulse2000, Pulse2050 and Pulse2100) or κ is greater or equal to 5 x 10^{-7} m^2/s, a significant percent of the GHSZ will be lost before the GHSZ volume rebounds to post-perturbation seafloor temperatures. The range of integrations carried out here demonstrates that the typical response timescale of the GHSZ and the timescale of CO_2 drawdown are of the same order when using realistic CO_2 drawdown scenarios and values of κ. This implies that the fiuture evolution of the GHSZ will depend strongly on the rate of uptake of anthropogenic CO_2 by the ocean.

Potential sea level change in response to melting ice sheets is not projected to impact the evolution of the global GHSZ significantly, even for the worst case scenario in which both the Greenland Ice Sheet and the WAIS melt completely within the next millenia.

The results presented here suggest that the marine hydrate reservoir may be affected significantly by future atmospheric greenhouse gas increases, with the GHSZ response varying in timing and intensity as a function of projected climate change. The initial response of the GHSZ to increases in anthropogenically-sourced atmospheric CO_2 occurs after $\sim$200 years of model integration (i.e. year 2050) and the global GHSZ continues to respond over 5-40 kyr to this forcing. Effects of GHSZ loss, including emissions of hydrate bound carbon to the exogenic carbon cycle, may therefore be felt within centuries and last for tens of thousands of years.

References

K.K. Andersen, N. Azuma, J.-M. Barnola, M. Bigler, P. Biscaye, N. Caillon, J. Chappellaz, H.B. Clausen, D. Dahl-Jensen, H. Fischer, J. Flückiger, D. Fritzsche, Y. Fujii, K. Goto-Azuma, K. Grnvold, N.S. Gundestrup, M. Hansson, C. Huber, C.S. Hvidberg, S.J. Johnsen, U. Jonsell, J. Jouzel, S. Kipfstuhl, A. Landais, M. Leuenberger, R. Lorrain, V. Masson-Delmotte, H. Miller, H. Motoyama, H. Narita, T. Popp, S.O. Rasmussen, D. Raynaud, R. Rothlisberger, U. Ruth, D. Samyn, J. Schwander, H. Shoji, M.-L. Siggard-Andersen, J.P. Steffensen, T. Stocker, A.E. Sveinbjörnsdóttir, A. Svensson, M. Takata, J.-L. Tison, T. Thorsteinsson, O. Watanabe, F. Wilhelms, and J. W. C. White. High-resolution record of Northern Hemisphere climate extending into the last interglacial period. *Nature*, 431:147–151, 2004.

D. Archer and B. Buffett. Time-dependent response of the global ocean clathrate reservoir to climatic and anthropogenic forcing. *Geochemistry Geophysics Geosystems*, 6, 2005.

D. Archer and A. Ganopolski. A movable trigger: Fossil fuel CO_2 and the onset of the next glaciation. *Geochemistry Geophysics Geosystems*, 6, 2005.

L. Augustin, C. Barbante, P.R.F. Barnes, J.M. Barnola, M. Bigler, E. Castellano, O. Cattani, J. Chappellaz, D. Dahl-Jensen, B. Delmonte, G. Dreyfus, G. Durand, S. Falourd, H. Fischer, J. Flückiger, M.E. Hansson, P. Huybrechts, G. Jugie, S.J. Johnsen, J. Jouze, P. Kaufmann, J. Kipfstuhl, F. Lambert, V.Y. Lipenkov, G.C. Littot, A. Longinelli, R. Lorrain, V. Maggi, V. Masson-Delmotte, H. Miller, R. Mulvaney, J. Oerlemans, H. Oerter, G. Orombelli, F. Parrenin, D.A. Peel, J. Petit, D. Raynaud, C. Ritz, U. Ruth, J. Schwander, U. Siegenthaler, R. Souchez, B. Stauffer, J.P. Steffensen, B. Stenni, T.F. Stocker, I.E. Tabacco1, R. Udisti, R.S.W. van de Wall, M. van den Broeke, J. Weiss, F. Wilhelms, J. Winther, and E.W. Wolff andM. Zucchelli. Eight glacial cycles from an Antarctic ice core. *Nature*, 429:623–628, 2004.

N.L.B. Bangs, R.J. Musgrave, and A.M. Tréhu. Upward shifts in the southern Hydrate Ridge gas hydrate stability zone following postglacial warming, offshore Oregon. *Journal of Geophysical Research*, 110, 2005.

T.P. Barnett, D.W. Pierce, K.M. AchutaRao, P.J. Gleckler, B.D. Santer, J.M. Gregory, and W.M. Washington. Penetration of human-induced warming into the world's oceans. *Science*, 309:284–287, 2005.

K.L. Bice and J. Marotzke. Could changing ocean circulation have destabilized methane hydrate at the Paleocene/Eocene boundary? *Paleoceanography*, 17, 2002.

C.M. Bitz, M.M. Holland, A.J. Weaver, and M. Eby. Simulating the ice-thickness distribution in a coupled climate model. *Journal of Geophysical Research*, 106:2441–2464, 2001.

K.M. Brown, N.L. Bangs, P.N. Froelich, and K.A. Kvenvolden. The nature, distribution, and origin of gas hydrate in the Chile Triple Junction. *Earth and Planetary Science Letters*, 139:471–483, 1996.

K. Bryan and L. Lewis. A water mass model of the world ocean. *Journal of Geophysical Research*, 84:311–337, 1979.

B. Buffett and D. Archer. Global inventory of methane clathrate: sensitivity to changes in the deep ocean. *Earth and Planetary Science Letters*, 227:185–199, 2004.

M.B. Clennell. Permafrost-associated gas hydrate. In M.D. Max, editor, *Movement and Accumulation of Methane in Marine Sediments: Relation to Gas Hydrate Systems*, pages 105–122. Kluwer Academic Publishers, Boston, 2000.

T.S. Collett. Natural gas hydrate as a potential energy resource. In M.D. Max, editor, *Natural Gas Hydrate in Oceanic and Permafrost Environments*, pages 123–126. Kluwer Academic Publishers, Boston, 2000.

T.S. Collett and S.R. Dallimore. Permafrost-associated gas hydrate. In M.D. Max, editor, *Natural Gas Hydrate in Oceanic and Permafrost Environments*, pages 43–60. Kluwer Academic Publishers, Boston, 2001.

M. Cottet-Puinel, A.J. Weaver, C. Hillaire-Marcel, A. de Vernal, P.U. Clark, and M. Eby. Variation of Labrador Sea water formation over the last glacial cycle in a climate model of intermediate complexity. *Quaternary Science Reviews*, 23, 2004.

E.E. Davis and R.D. Hyndman. Rates of fluid expulsion across the Northern Cascadia Accretionary Prism: Constraints from new heat flow and multichannel seismic reflection data. *Journal of Geophysical Research*, 95:8869–8889, 1990.

G.R. Dickens. The potential volume of oceanic methane hydrates with variable external conditions. *Organic Geochemistry*, 32:1179–1193, 2001.

G.R. Dickens. Rethinking the global carbon cycle with a large, dynamic and microbially mediated gas hydrate capacitor. *Earth and Planetary Science Letters*, 213:169–183, 2003.

G.R. Dickens, M.M. Castillo, and J.C.G. Walker. A blast of gas in the latest Paleocene: Simulating first-order effects of massive dissociation of oceanic methane hydrate. *Geology*, 25:259–262, 1997.

G.R. Dickens and M.S. Quinby-Hunt. Methane hydrate stability in seawater. *Journal of Geophysical Research*, 21:2115–2118, 1994.

G.R. Dickens and M.S. Quinby-Hunt. Methane hydrate stability in pore water: A simple theoretical approach for geophysical applications. *Journal of Geophysical Research*, 102: 773–783, 1997.

T.L. Ewen, A.J. Weaver, and M. Eby. Sensitivity of the inorganic ocean carbon cycle to future climate warming in the UVic coupled model. *Atmosphere-Ocean*, 42:23–42, 2004.

J.P. Foucher, H. Nouze, and P. Henry. Observation and tentative interpretation of a double BSR on the Nankai slope. *Marine Geology*, 187:161–175, 2002.

P.R. Gent and J.C. McWilliams. Isopycnal mixing in ocean circulation models. *Journal of Physical Oceanography*, 20:150–155, 1990.

D.S. Goldberg, T.S. Collett, and R.D. Hyndman. Ground truth: in-situ properties of hydrate. In M.D. Max, editor, *Natural Gas Hydrate in Oceanic and Permafrost Environments*, pages 123–126. Kluwer Academic Publishers, Boston, 2000.

V. Gornitz and I. Fung. Potential distribution of methane hydrates in the world's oceans. *Global Biogeochemical Cycles*, 8:335–347, 1994.

L.D.D. Harvey and Z. Huang. Evaluation of the potential impact of methane clathrate destabilization on future warming. *Journal of Geophysical Research*, 100:2905–2926, 1995.

J.T. Houghton, Y. Ding, D.J. Griggs, M. Noguer, P.J. Van der Linden, X. Dai, K. Maskell, and C.A. Johnson, editors. *Climate change 2001: the scientific basis. IPCC Third Assessment Report.* Cambridge University Press, Cambridge, UK, 2001.

E. C. Hunke and J. K. Dukowicz. An elastic-viscous-plastic model for sea ice dynamics. *Journal of Physical Oceanography*, 27:1849–1867, 1997.

R. Hyndman, K. Wang, T. Yuan, and G. Spence. Tectonic sediment thickening, fluid expulsion, and the thermal regime of subduction zone accretionary prisms: the Cascadia Margin off Vancouver Island. *Journal of Geophysical Research*, 98:21865–21876, 1993.

R.D. Hyndman and E.E. Davis. A mechanism for the formation of methane hydrate and sea-floor bottom-simulating reflectors by vertical fluid expulsion. *Journal of Geophysical Research*, 97:7025–7041, 1992.

R.D. Hyndman and G.D. Spence. A seismic study of methane hydrate marine bottom simulating reflectors. *Journal of Geophysical Research*, 97:6683–6698, 1992.

M.E. Katz, B.S. Cramer, G.S. Mountain, S. Katz, and K.G. Miller. Uncorking the bottle: What triggered the Paleocene/Eocene thermal maximum methane release? *Paleoceanography*, 16:549–562, 2001.

J. Kennett. *Marine Geology.* Prentice-Hall, New Jersey, 2003.

J.P. Kennett, K.G. Cannariato, I.L. Hendy, and R.J. Behl. *Methane Hydrates in Quaternary Climate Change: the Clathrate Gun Hypothesis.* American Geophysical Union, Washington, DC, 2003.

J.P. Kennett and L.D. Stott. Abrupt deep-sea warming, palaeoceanographic changes and benthic extinctions at the end of the Palaeocene. *Nature*, 353:225–229, 1991.

J.B. Klauda and S.I. Sandler. Phase behavior of clathrate hydrates: a model for single and multiple gas component hydrates. *Chemical Engineering Science*, 58:27–41, 2002.

J.B. Klauda and S.I. Sandler. Global distribution of methane hydrate in ocean sediment. *Energy & Fuels*, 19:459–470, 2005.

K.A. Kvenvolden. Gas hydrates - geological perspective and global change. *Reviews of Geophysics*, 31:173–187, 1993.

K.A. Kvenvolden. A primer on the geological occurrence of gas hydrate. In J.P. Henriet and J. Mienert, editors, *Gas Hydrates: Relevance to world margin stability and climatic change*, pages 9–30. Geological Society Special Publications, London, 1998.

G.J. De Lange and H.-J. Brumshack. The occurrence of gas hydrates in Eastern Mediterranean mud dome structures as indicated by pore-water composition. In J.P. Henriet and J. Mienert, editors, *Gas Hydrates: Relevance to world margin stability and climatic change*, pages 9–30. Geological Society Special Publications, London, 1998.

S. Levitus. Climatological atmas of the world ocean. Technical Report 13, Natl. Oceanic and Atmos. Admin, Silver Spring, Md., 1982.

J.P. Lewis, A.J. Weaver, S.T. Johnston, and M. Eby. Neoproterozoic "snowball Earth": Dynamic sea ice over a quiescent ocean. *Paleoceanography*, 18:1092, 2003.

M. Maslin, M. Owen, S. Day, and D. Long. Linking continental-slope failures and climate change: Testing the clathrate gun hypothesis. *Geology*, 32:53–56, 2004.

H.D. Matthews, A.J. Weaver, K.J. Meissner, N.P. Gillett, and M. Eby. Natural and anthropogenic climate change: incorporating historical land cover change, vegetation dynamics and the global carbon cycle. *Climate Dynamics*, 22:461–479, 2003.

K. J. Meissner, A. Schmittner, A. J. Weaver, and J. F. Adkins. Ventilation of the North Atlantic Ocean during the Last Glacial Maximum: A comparison between simulated and observed radiocarbon ages. *Paleoceanography*, 18:1023, 2003.

J. Mienert, M. Vanneste, K. Andreassen, H. Haflidason, and H.P. Sejrup. Ocean warming and gas hydrate stability on the mid-Norwegian margin at the Storegga Slide. *Marine and Petroleum Geology*, 22:233–244, 2005.

A.V. Milkov. Global estimates of hydrate-bound gas in marine sediments: how much is really out there? *Earth-Science Reviews*, 66:183–197, 2004.

A.V. Milkov and R. Sassen. Thickness of the gas hydrate stability zone, Gulf of Mexico continental slope. *Marine and Petroleum Geology*, 17:981–991, 2000.

J.J. Miller, M.W. Lee, and R. von Huene. An analysis of a seismic reflection from the base of the gas hydrate zone, offshore Peru. *AAPG Bulletin*, 75:910–924, 1991.

J.F. Mitchell, T.C. Johns, J.M. Gregory, and S.F. Tett. Climate response to increasing levels of greenhouse gases and sulphate aerosols. *Nature*, 376:501–504, 1995.

N. Nakićenović, O. Davidson, G. Davis, A. Grübler, T. Kram, E. Lebre La Rovere, B Metz, T. Morita, W. Pepper, H. Pitcher, A. Sankovski, P. Shukla, R Swart, R. Watson, and Z. Dadi, editors. *IPCC Special Report: Emissions Scenarios.* Intergovernmental Panel on Climate Change, 2000.

R. Pacanowski. *MOM 2 Documentation User's Guide and Reference Manual, GFDL Ocean Group Technical Report.* NOAA/GFDL, Princeton, 1995.

E.T. Peltzer and P.G. Brewer. Practical physical chemistry and empirical predictions of methane hydrate stability. In M.D. Max, editor, *Natural Gas Hydrate in Oceanic and Permafrost Environments*, pages 17–28. Kluwer Academic Publishers, Boston, 2000.

J.R. Petit, J. Jouzel, D. Raynaud, N.I. Barkov, J-.M. Barnola, I. Basile, M. Benders, J. Chappellaz, M. Davis, G. Delague, M. Delmotte, V.M. Kotlyakov, M. Legrand, V.Y. Lipenkov, C. Lorius, L. Pépin, C. Ritz, E. Saltzman, and M. Stievenard. Climate and atmospheric history of the past 420,000 years from the Vostok ice core, Antarctica. *Nature*, 399:429–436, 1999.

J.W. Pohlman, E.A. Canuel, G.D. Spence, M.J. Whiticar, and R.B. Coffin. The origin of thermogenic gas hydrates on the northern Cascadia Margin as inferred from isotopic (c-13/c-12 and D/H) and molecular composition of hydrate and vent gas. *Organic Geochemistry*, 36:703–716, 2005.

H.N. Pollack, S.J. Hurter, and J.R. Johnson. Heat flow from the Earth's interior: analysis of the global data set. *Reviews of Geophysics*, 31:267–280, 1993.

J. Ridley, P. Huybrechts, J.M. Gregory, and J.A. Lowe. Future changes in the Greenland ice sheet: A 3000 year simulation with a high resolution ice sheet model interactively coupled to an AOGCM. *Journal of Climate*, 2005. in press.

R. Sassen, S.T. Sweet, A.V. Milkov, D.A. DeFreitas, and M.C. Kennicutt. Thermogenic vent gas and gas hydrate in the Gulf of Mexico slope: is gas hydrate decomposition significant? *Geology*, 29:107–110, 2005.

A. Schmittner, K. J. Meissner, M. Eby, and A. J. Weaver. Forcing of the deep ocean circulation in simulations of the Last Glacial Maximum. *Paleoceanography*, 17, 2002.

J.P. Severinghaus, T. Sowers, E.J. Brook, R.B. Alley, and M.L. Bender. Timing of abrupt climate change at the end of the Younger Dryas interval from thermally fractionated gases in polar ice. *Nature*, 391:141–146, 1998.

E.D. Sloan. Physical/chemical properties of gas hydrates and application to world margin stability and climatic change. In J.P. Henriet and J. Mienert, editors, *Gas Hydrates: Relevance to world margin stability and climatic change*, pages 9–30. Geological Society Special Publications, London, 1998.

E.D. Sloan. Fundamental principles and applications of natural gas hydrates. *Nature*, 426: 353–359, 2003.

V.A. Soloviev. Global estimation of gas content in submarine gas hydrate accumulations. *Russian Geology and Geophysics*, 43:609–624, 2002.

R.J. Stouffer and S. Manabe. Equilibrium response of thermohaline circulation to large changes in atmospheric CO_2 circulation. *Climate Dynamics*, 20:759–773, 2003.

N. Sultan, P. Cochonat, J.-P. Foucher, and J. Mienert. Effect of gas hydrates melting on seafloor slope instability. *Marine Geology*, 213:379–401, 2004.

H. Svensen, S. Planke, A. Malthe-Sørenssen, B. Jamtveit, R. Myklebust, T.R. Eidem, and S.S. Rey. Release of methane from a volcanic basin as a mechanisms for initial Eocene warming. *Nature*, 429:542–544, 2004.

D.L. Turcotte and G. Schubert. *Geodynamics Applications of Continuum Physics to Geological Problems.* John Wiley, New York, 1982.

A. J. Weaver. The UVic Earth System Climate Model and the thermohaline circulation in past, present and future climates. *The State of the Planet: Frontiers and Challenges in Geophysics, IUGG and AGU Geophysical Monograph Series*, 150:279–296, 2004.

A.J. Weaver, P.B. Duffy, M. Eby, and E.C. Wiebe. Evaluation of ocean and climate models using present-day observations and forcing. *Atmosphere Ocean*, 38:271–301, 2000.

A.J. Weaver, M. Eby, E.C. Weibe, C.M. Bitz, P.B. Duffy, T.L. Ewen, A.F. Fanning, M.M. Holland, A. MacFadyen, H.D. Matthews, K.J. Meissner, O. Saenko, A. Schmittner, H. Wang, and M. Yoshimori. The UVic Earth System Climate Model: Model description, climatology and application to past, present and future climates. *Atmosphere Ocean*, 39: 361–428, 2001.

J.L. Weinberger, K.M. Brown, and P.E. Long. Painting a picture of gas hydrate distribution with thermal images. *Geophysical Research Letters*, 32, 2005.

E.C. Wiebe and A.J. Weaver. On the sensitivity of global warming experiments to the parameterization of sub-grid scale ocean mixing. *Climate Dynamics*, 15:875–893, 1999.

W. Xu, R.P. Lowell, and E.T. Peltzer. Effect of seafloor temperature and pressure variations on methane flux from a gas hydrate layer: Comparisons between current and late Paleocene conditions. *Journal of Geophysical Research*, 106:26413–26423, 2001.

W. Xu and C Ruppel. Predicting the occurrence, distribution, and evolution of methane gas hydrate in porous marine sediments. *Journal of Geophysical Research*, 104:5081–5095, 1999.

J.C. Zachos, M.W. Wara, S. Bohaty, M.L. Delaney, M.R. Petrizzo, A. Brill, T.J. Bralower, and I. Premoli-Silva. A transient rise in tropical sea surface temperature during the Paleocene-Eocene Thermal Maximum. *Science*, 302:1551–1554, 2003.